



## ANNALS OF THE NEW YORK ACADEMY OF SCIENCES

Special Issue: *The Year in Climate Science Research*

REVIEW

# Hydrological cycle changes under global warming and their effects on multiscale climate variability

Jian Ma,<sup>1</sup> Lei Zhou,<sup>1,2</sup> Gregory R. Foltz,<sup>3</sup> Xia Qu,<sup>4</sup> Jun Ying,<sup>5</sup> Hiroki Tokinaga,<sup>6</sup> Carlos R. Mechoso,<sup>7</sup> Jinbao Li,<sup>8</sup> and Xingyu Gu<sup>9</sup>

<sup>1</sup>School of Oceanography, Shanghai Jiao Tong University, Xuhui, Shanghai, China. <sup>2</sup>Southern Marine Science and Engineering Guangdong Laboratory (Zhuhai), Sun Yat-sen University, Guangzhou, China. <sup>3</sup>Atlantic Oceanographic and Meteorological Laboratory, NOAA, Miami, Florida. <sup>4</sup>Center for Monsoon System Research and State Key Laboratory of Numerical Modeling for Atmospheric Sciences and Geophysical Fluid Dynamics, Institute of Atmospheric Physics, Chinese Academy of Sciences, Beijing, China. <sup>5</sup>State Key Laboratory of Satellite Ocean Environment Dynamics, Second Institute of Oceanography, Ministry of Natural Resources, Hangzhou, Zhejiang, China. <sup>6</sup>Research Institute for Applied Mechanics, Kyushu University, Kasuga, Fukuoka, Japan. <sup>7</sup>Department of Atmospheric and Oceanic Sciences, University of California, Los Angeles, Los Angeles, California. <sup>8</sup>Department of Geography, University of Hong Kong, Pokfulam, Hong Kong SAR, China. <sup>9</sup>College of Marine Sciences, Shanghai Ocean University, Pudong, Shanghai, China

Address for correspondence: Jian Ma, School of Oceanography, Shanghai Jiao Tong University, Xuhui, Shanghai 200030, China. Jian.Ma@SJTU.edu.cn

Despite a globally uniform increase in the concentrations of emitted greenhouse gases, radiatively forced surface warming can have significant spatial variations. These define warming patterns that depend on preexisting climate states and through atmospheric and oceanic dynamics can drive changes of the hydrological cycle with global-scale feedbacks. Our study reviews research progress on the hydrological cycle changes and their effects on multiscale climate variability. Overall, interannual variability is expected to become stronger in the Pacific and Indian Oceans and weaker in the Atlantic. Global monsoon rainfall is projected to increase and the wet season to lengthen despite a slowdown of atmospheric circulation. Strong variations among monsoon regions are likely to emerge, depending on surface conditions such as orography and land–sea contrast. Interdecadal climate variability is expected to modulate the globally averaged surface temperature change with pronounced anomalies in the polar and equatorial regions, leading to prolonged periods of enhanced or reduced warming. It is emphasized that advanced global observations, regional simulations, and process-level investigations are essential for improvements in understanding, predicting, and projecting the modes of climate variability, monsoon sensitivity, and energetic fluctuations in a warming climate.

**Keywords:** global warming; climate change; hydrological cycle; climate variability; trend uncertainty

## Introduction

Climate provides the environment for all living creatures on Earth, and its variability has tremendous impacts on entire aspects of human society. The impacts induced by marked changes in the long-term mean climate and its variability have been well acknowledged by scientists and the general public. Global land and ocean warming poses severe stresses to the hydrological, ecological, and social environment upon which human beings are dependent, especially in the tropics. Outstanding

footprints of climate change are the increased occurrence of extreme weather events, global-scale glacier melting, and the consequent sea-level rise. The United Nations Intergovernmental Panel on Climate Change (IPCC) has evaluated global and regional climate change based on extensive research. The Fifth Assessment Report (AR5) of the IPCC indicates that although the increase in greenhouse gas (GHG) concentrations is approximately uniform in the atmosphere, surface warming exhibits significant spatial nonuniformity<sup>1</sup> and regional diversity<sup>2</sup> (Fig. 1).

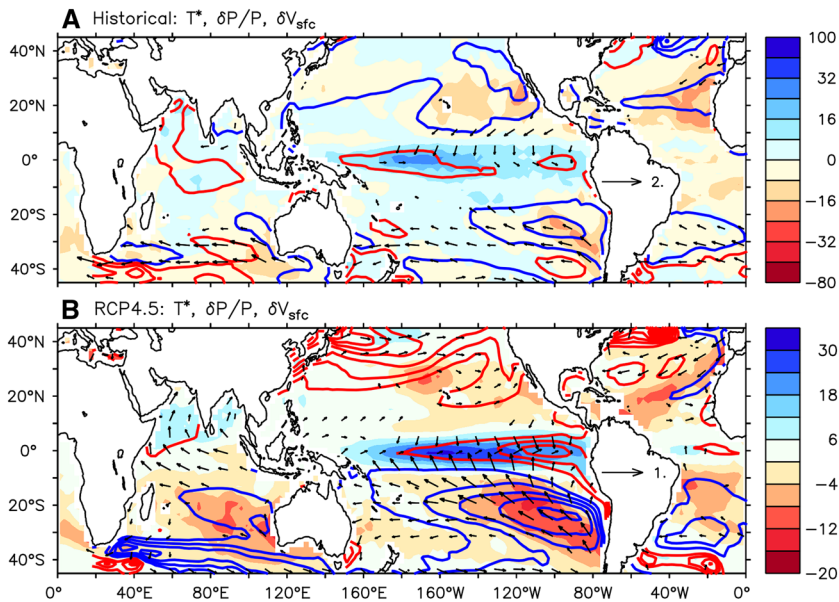


**Figure 1.** Relationship between ensemble and annual mean regional changes of the tropical SST (contours, K), 1000 hPa winds (vectors, m/s), and precipitation in percentage (color shading, %) projected by 37 CMIP5 models. The forcing scenarios include (A) historical with the difference between means of 1901–1910 and 1991–2000, and (B) RCP4.5 with 2089–2098 minus 2006–2015. All changes are normalized by the tropical (20°S–20°N) mean SST warming.

Global climate change is geographically heterogeneous. The signature of multiscale changes in the mean and variability of climate properties, such as air/sea temperatures, circulation, and rainfall, differs among regions. Long-term trends may even have opposite signs in adjacent areas due to coupling mechanisms, such as land–sea and air–sea interactions. Therefore, for a specific area, regional climate change, that is, the deviation from a large-scale average for the area, can be more important than global mean trends, from both a scientific and a socioeconomic viewpoint.<sup>1–4</sup> Moreover, regional changes usually leave footprints in other regions and may have global impacts because the whole climate system is fully connected across spatial and temporal scales.<sup>5–7</sup>

The increases in surface temperature, comprising both land and sea surface temperature (SST) and often used as one indicator of the climate state, are not uniform over the globe. The primary focus of the present study is on SST, which has been the subject of many analyses and reanalyses. Discrepancies are still discernible between many of these different studies, as recently diagnosed in Ref. 8. Some uncertainties in scientific findings seem

to stem from the uncertainties in different data sources.<sup>9</sup> Nevertheless, there is a strong consensus that SST has increased almost everywhere in the oceans in the 20th century except for the northern Atlantic.<sup>10–12</sup> The largest SST increase occurred in the midlatitudes of the Northern and Southern Hemispheres.<sup>13–15</sup> However, SST trends have been found to be inconsistent in the eastern Pacific in both observations and simulations,<sup>16,17</sup> especially in the region known as the equatorial cold tongue (Fig. 1). Regional discrepancies between warming<sup>18,19</sup> and cooling<sup>20,21</sup> result in uncertainties in the trends of the zonal SST gradient between the eastern and western parts of the basin. This leads to different conclusions on the projections of changes of the Walker circulation in the atmosphere and the El Niño–Southern Oscillation (ENSO)<sup>22–25</sup> in the context of global warming.

Moreover, there are areas that have seemingly cooled even in the Southern Hemisphere despite pronounced global warming in past few decades.<sup>26–28</sup> This has been attributed to the uncertainty in trend analysis due to the combined effects of the Southern Annular Mode (SAM) over the Antarctic, the Southern Oscillation beyond the

polar region, and El Niño in the tropics.<sup>29–31</sup> SST changes over the coastal regions are more uneven than in the open oceans.<sup>32</sup> Climate extremes (e.g., cold/heat waves and flood/drought events) have exhibited heterogeneous trends across many regions. These complexities make it challenging to clearly understand and reliably project regional climate change and the associated responses of climate variability.

The uncertainty in climate projections has been largely attributed to the high sensitivity of climate models to the parameterizations for which the fundamental physics and dynamics are still poorly understood, such as cloud and radiative transfer (e.g., Refs. 33–35). Clouds interact with the large-scale environment in ways that are not fully known because atmospheric convection and large-scale circulation determine the distribution of water vapor throughout the whole air column. Latent heat released by phase changes of water is a major source of energy that drives and sustains the mean climate and its variability.<sup>36–38</sup> The vertical profiles of moisture and atmospheric heating are not only key dynamical and thermodynamic factors, but also essential elements for climate simulation, prediction, and projection.

In the tropics, the atmosphere is in a state of conditional instability. The concept of convective quasi-equilibrium is the basis for many widely used convection schemes in climate models.<sup>39–41</sup> Details of the interactions between large-scale circulation and small-scale convection that define different flavors of convective parameterization are beyond the scope of this review. The complexity of such interactions intrinsically affects the abilities of climate models to simulate the hydrological cycle and its changes, which alter convection and clouds. Based on the simulation results of multi-model ensembles and extensive diagnostic studies, a consensus has emerged that the dominant source of uncertainty in climate models is cloud change-associated convective and radiative feedback, which leads to poor performance in simulating precipitation.<sup>42–46</sup>

Global warming-induced changes in the processes that modulate the convective and radiative feedbacks and their effects on the hydrological cycle (see below) are key elements of the responses of climate variability.<sup>47</sup> With the increase in tropospheric temperature and rise of the tropopause,<sup>48</sup> the pro-

files of most atmospheric variables shift upward but are tuned by the atmosphere circulation that is also modified by the global warming. Models show that atmospheric warming also leads to increased water vapor, decreased lapse rate, and slowed large-scale circulation, which can contribute either positively or negatively to changes in evaporation, divergence, convection, and precipitation.<sup>49</sup> For instance, low-level moisture increase under global warming would enhance convective activities, causing the rich-get-richer pattern in rainfall change.<sup>50</sup> However, gross moist stability tends to increase and counteract the rich-get-richer pattern in the tropics, consistent with the weakening of tropical circulation.<sup>51</sup> Another robust response is an expansion of the Hadley cell<sup>52</sup> due to static stabilization of the tropical atmosphere.<sup>53</sup> Regional precipitation redistribution is further modulated by the SST pattern change and associated feedbacks with the atmospheric circulation.<sup>54</sup> This interdependence can drastically influence<sup>55</sup> future climate variability, such as the ENSO, the Indian Ocean Dipole (IOD), and monsoon circulations. Observed and predicted changes in climate variability have been investigated substantially,<sup>47,56–58</sup> and yet understanding and constraining uncertainty in climate projections remain difficult challenges.<sup>59,60</sup>

The present study aims to review changes in the hydrological cycle and their effects on various important climate processes on different timescales, such as the ENSO, global and regional monsoon systems, and the Atlantic multidecadal oscillation (AMO). Our efforts intend to address specific points in the IPCC reports and not to replace them. We start by briefly summarizing the fundamental dynamics and general phenomena of regional climate change in “Important highlights of regional climate change” section. Multiscale climate variability and its responses to global warming are next reviewed along with the interactions among them. Interannual variability is addressed in “Influence on interannual variability” section; the monsoon systems are discussed in “Impact on monsoons” section; the relationships between global warming and interdecadal variability, such as the interdecadal Pacific oscillation (IPO), are examined in “Interdecadal variability and global warming” section. Finally, conclusions and indicative suggestions for future research are provided in “Discussion and outlook” section.

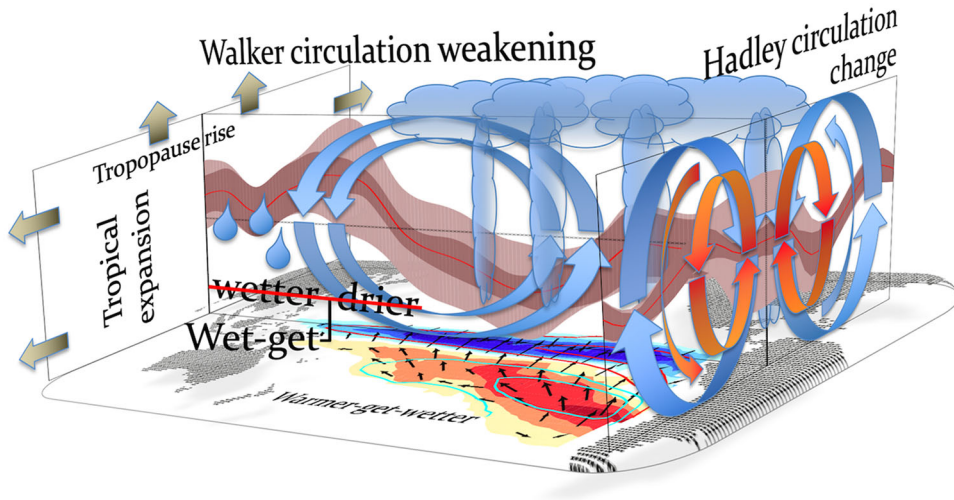


**Figure 2.** Schematic plot for regional climate change in the tropics. The wet-get-wetter/drier represents the opposing effects on rainfall change between the atmospheric moistening and circulation weakening, with the red bar across denoting their offset. The warmer-get-wetter paradigm is illustrated with ensemble mean changes of SST (contours), precipitation (shading), and surface winds (vectors) in 19 CMIP5 simulations (adapted from Ref. 61). Changes of the Hadley (500-hPa zonal-integrated meridional streamfunction) and Walker (15°S–15°N averaged 250-hPa velocity potential) cells are reproduced from Ref. 62, with ensemble means (red line) accompanied by spreads ( $\pm$  standard deviation) of 22 CMIP3 models (light red shading) and those without the first two modes in singular value decompositions on SST (dark red shading), where red (blue) circles represent strengthening (weakening) circulations.

### Important highlights of regional climate change

Regional climate change (Fig. 1) includes the spatial patterns in the responses to the increase in GHG concentrations of land/SST, precipitation, atmospheric and ocean circulations, water vapor, clouds, hydrological cycle, and energy transport.<sup>49</sup> These regional manifestations of climate change influence the distribution of heat waves, storminess, droughts, floods, and wildfires, all of which affect fisheries, agriculture and food security, the economy, and ecosystem sustainability.<sup>59</sup> In a broad sense, we will label regional to climate phenomena in scales ranging from thousands of kilometers (continents and ocean basins) to tens of kilometers (ocean currents and eddies). This section introduces the fundamental mechanisms<sup>61,62</sup> shaping regional climate change in the tropics (Fig. 2) and compares the responses of different ocean basins with global warming (Fig. 1).

#### *Dynamical fundamentals of tropical climate change*

Tropical SST change can be decomposed<sup>63</sup> into a spatial average (uniform increase) and devia-

tions from it (regional patterns). A hypothetical uniform SST warming would result in increased atmospheric water vapor and static stability as tropospheric warming increases with height.<sup>53</sup> Regional consequences can include an expansion of the tropics,<sup>52</sup> a slowdown of the atmospheric circulation,<sup>51</sup> and an increase in the precipitation minus evaporation ( $P-E$ ) gradient.<sup>64</sup> Recent studies suggest that under global warming, the spatial patterns of SST can change significantly, affecting interactions between the ocean and atmosphere.<sup>62</sup> This has been recognized as a dominant factor and source of uncertainty in water cycle<sup>63</sup> and oceanic rainfall<sup>62</sup> changes caused by the adjustments of atmospheric circulation.<sup>53</sup> Such robust changes are illustrated in Figure 2. On the other hand, amplified land warming by enhanced longwave heating by CO<sub>2</sub><sup>65</sup> and water vapor<sup>66</sup> and the resultant reduction of relative humidity<sup>67</sup> dominate the rainfall and circulation changes over land.

**Spatially uniform SST warming.** Observational evidence shows that the subsidence boundaries of the tropics are expanding poleward in both hemispheres, based on at least five metrics:

tropopause height frequency; satellite-observed outgoing longwave radiation, atmosphere temperature, and cloud cover; extent of Hadley cell stream function; latitudinal location of jet streams; and precipitation intensity.<sup>68</sup> However, the most easily observed metrics (e.g., precipitation) have too strong surface forcing, while the most closely related parameters (e.g., stream function) are not always directly observable. Hence, the estimated expansion rate varies widely from 0.5° to 1.0° per decade. Stratospheric ozone depletion, GHG concentration increase, and aerosol emission all contribute to tropical widening, and attribution is complicated by their high internal variability.<sup>69</sup> Model diagnostics also reveal significant uncertainty induced by contradictory radiative effects of cloud and water vapor changes.<sup>70</sup>

Tentative physical explanations for the tropical expansion have been given based on either numerical simulations or theoretical predictions. Static stabilization of the tropical atmosphere reduces the baroclinicity in the subtropics and displaces eddy activity to higher latitudes.<sup>52</sup> Phase speed increase of upper tropospheric baroclinic waves<sup>71</sup> weakens the waves' equatorward penetration, which shifts the jet stream by altering eddy momentum flux convergence associated with the storm tracks. The stratospheric circumpolar westerly jet reinforces the tropical expansion in a similar way.<sup>72</sup> Aerosols are also found to help reduce meridional temperature gradients, weakening and expanding the meridional stream function and zonal wind patterns.<sup>69</sup> Held and Hou developed a simplified framework to derive the latitudinal boundary of the Hadley circulation as a function of tropopause height, with a tropopause rise predicting Hadley cell expansion.<sup>48</sup> This process involves relaxed meridional temperature gradients, which can be traced back to a reduced vertical shear of the zonal wind through the thermal wind relation.<sup>53</sup>

The weakening tropical circulation is then connected to the increased depth of convection, as constrained by conservation of moist static energy.<sup>73</sup> Such a slowdown (Fig. 2) was initially observed for the Walker cell<sup>74</sup> in association with reduced gradients of sea-level pressure,<sup>16</sup> although this trend is partially offset<sup>75</sup> for global mean surface wind speed.<sup>76</sup> The reduction in strength of both the ascent and descent branches has been explained on the basis of thermodynamic<sup>51</sup> and

radiative relationships<sup>77</sup> in model projections. The global mean water vapor and vertical gradient of air temperature increase at  $\sim 7\% \text{ K}^{-1}$  of surface warming, but the fractional changes in global mean precipitation and net longwave radiative cooling are only  $\sim 1\text{--}2\% \text{ K}^{-1}$ . These facts combined indicate a weakening of the circulation at a rate of about  $5\% \text{ K}^{-1}$ , though why precipitation changes as such has not been thoroughly explained from surface energy and evaporation points of view.<sup>49</sup>

The moistened boundary layer becomes moist unstable under global warming, which would enhance convection and precipitation in convective regions, as indicated in Chapter 14 of IPCC AR5. This is known as the dynamical rich-get-richer view.<sup>78</sup> As the overall stability increases and circulation weakens, however, the tropics-wide rich-get-richer pattern cannot hold, although it may be able to locally. Meanwhile, in the assumed absence of circulation changes, increased atmospheric water vapor implies an increased moisture transport from dry to wet regions and an increased gradient of  $P\text{--}E$ . This thermodynamic wet-get-wetter view<sup>51</sup> appears to hold on very large spatial scales.

However, neither observations nor simulations support the rich-get-richer or wet-get-wetter argument regionally throughout the whole tropics: the spatial correlation between climatological precipitation and future change is low in the projections of the Coupled Model Intercomparison Project (CMIP) phase 5.<sup>79</sup> An upped-ante hypothesis was proposed to explain rainfall reduction in the convective margins.<sup>50</sup> However, this mechanism does not apply universally in all margins but only in those where moisture increase is insufficient to meet the raised convective threshold following the tropical mean SST warming.<sup>80</sup> These discrepancies emphasize the need for spatially consistent theories to explain regional change of tropical precipitation.

**SST pattern effect.** The slowdown of circulation induced by global warming can manifest itself locally through a dynamical mechanism<sup>53</sup> dubbed mean advection of stratification change (MASC). A tropics-wide atmospheric stabilization (increased warming with height) leads to an elevated maximum warming in the troposphere resulting in relative cooling of the air column in ascending regions due to anomalous cold advection

of low-level air, and relative warming in subsidence regions due to warm advection. This not only reduces horizontal air temperature and pressure gradients as well as vertical velocity, but also causes the greatest future weakening of the circulation to occur in the region with the strongest preexisting motion.<sup>49</sup> Therefore, MASC exerts a wet-get-drier effect on regional precipitation (Fig. 2), opposing and mitigating wet-get-wetter.<sup>54</sup>

Due to the complexity of climate feedbacks and the differences in ocean–atmosphere interactions,<sup>81</sup> surface warming from the greenhouse effect is significantly enhanced in some regions<sup>82</sup> (e.g., the equatorial Pacific) and notably weakened in others. The offset between wet-get-wetter and wet-get-drier allows for the deviations of SST warming from its tropical mean to dominate regional rainfall change, and precipitation increases where there is more warming and decreases where there is less (Fig. 2). This warmer-get-wetter paradigm is organized into two outstanding modes (Fig. 1), both accompanied by coherent surface wind patterns. An equatorial peak in warming anchors a local increase in precipitation and anomalous convergence of surface winds, and a meridional dipole centered near the equator enhances rainfall and convergence and weakens the trade winds over the warmer hemisphere.

The SST patterns induce changes in the atmospheric circulation that have the same order of magnitude as the slowdown.<sup>49</sup> Both the Hadley and Walker circulations tend to weaken with spatially uniform SST warming; however, the Hadley cell slowdown is partially offset by the effect of the SST patterns. The two mechanisms reinforce each other in some regions but oppose in others, resulting in robust weakening north of the equator but weak and highly uncertain changes near and south of the equator (Fig. 2). Specifically, the equatorial peak of SST warming drives an enhanced Hadley circulation on either side of the equator, and the south-to-north gradient causes a cross-equatorial circulation, implying enhanced and weakened Hadley cells in the Southern and Northern Hemisphere, respectively. A strengthening trend has been documented for the Hadley cell in recent decades;<sup>83</sup> however, this trend seems to be largely due to internal variability.

Therefore, the spatially nonuniform SST warming has significant consequences on the atmospheric circulation<sup>62</sup> and spatial redistribution of

precipitation.<sup>79</sup> The SST patterns also act against the slowdown of surface winds, and a significant enhancement of trade winds in the southeastern subtropics results in an insignificant trend for global mean speed.<sup>75</sup> The complexity of such competing mechanisms brings great uncertainty into historical observational data sets<sup>84</sup> and future projections by climate models,<sup>62</sup> including the CMIP6.<sup>85</sup>

### *Interbasin comparison of robust changes in the upper and deeper ocean*

Previous research has attributed spatial variations in ocean warming mainly to differences in air–sea coupling modes and ocean circulation between various ocean basins.<sup>63</sup> Oceanic diffusivity, subduction, and advection can transmit sea-surface warming signals to the interior. Turbulent mixing induced by surface winds and waves spreads heat into the deep ocean, while the meridional overturning circulation more directly transports warm water from the surface to the abyssal ocean at high latitudes. There are large differences in deep ocean circulation among the ocean basins. As a result, the nonuniformity in temperature change at and below the subsurface is more pronounced than that at the surface. Here, we review the aforementioned regional climate change in detail by comparing various ocean basins and discussing the dominant mechanisms responsible for their differences.<sup>61</sup>

**The surface ocean.** In the Pacific Ocean (Fig. 1B), there is minimal warming in the southeastern subtropics, which is in sharp contrast with the strong warming and enhanced rainfall north of the equator. The projected El Niño–like pattern of SST change<sup>82</sup> anchors strong convergence of the meridional wind to cause a significant precipitation increase in the eastern equatorial Pacific, corresponding to a robust weakening of the surface Walker circulation. The SST and precipitation changes in the equatorial and South Atlantic are similar to those in the Pacific, following the warmer-get-wetter paradigm. However, the North Atlantic is significantly different from the North Pacific with respect to the magnitude of surface and subsurface warming. The northern subduction branch of the Atlantic meridional overturning circulation (AMOC) transports surface warming into the deep ocean, resulting in weaker upper layer but stronger lower layer warming compared with the nonoverturning Pacific.

The projected surface warming of the Indian Ocean is more pronounced in the northwest than in the southeast (Fig. 1B). This is attributed to a local ocean–atmosphere coupled mode. On the background of global warming, ocean currents are relaxed by the weakening of the equatorial westerly winds. The subsequent anomalous downwelling warms SST in the western tropical Indian Ocean, while anomalous upwelling of lower layer water cools SST off the Sumatra–Java coast. Precipitation changes accordingly, as the positive phase of the IOD appears more frequently.<sup>86</sup> However, recent studies suggest that this may be due to overestimated activity of the IOD in climate models, which is unlikely to emerge in nature.<sup>87</sup>

**The interior ocean.** Increase of the Pacific subsurface temperature is only evident for northern subtropical mode water that originates in a major ocean subduction region. Meanwhile, the Kuroshio Extension exhibits enhanced local warming two to three times faster than the global mean SST increase, known as a “hotspot.”<sup>88</sup> Here, the subtropical western boundary currents are accelerated by global warming and are able to carry more tropical water to midlatitudes and cause pronounced warming. The eddy-induced mixing and mode water subduction near the Kuroshio Extension can transmit the warming signals downward from ocean surface simultaneously, resulting in robust local subsurface warming.

In addition, the interannual variability of the hotspot hints at anomalous forcing from the atmosphere that influences the surface fluxes of moisture and energy, resulting in marine heat waves, such as the “blob.”<sup>89,90</sup> This regulates the location where the hotspots actually appear,<sup>91</sup> and, in turn, greatly affect the location of hurricane and typhoon activity. The mode water–induced weakening of the subtropical countercurrent may also be a factor in the nonuniform distribution of SST warming.<sup>92</sup> The subsurface Indian Ocean has insignificant warming signals and needs further investigation.

Although the hotspot phenomenon also occurs in the Atlantic near the Gulf Stream, subsurface warming of the subtropical Atlantic is weaker than in the tropics and at high latitudes.<sup>61</sup> Leading to variations in ocean circulation,<sup>93</sup> subsurface warming is negatively correlated with thermocline depth,

which is symmetric between the tropical North and South Atlantic. This may also be the dominant reason for the meridionally symmetric responses of SST, precipitation, and surface winds to global warming, which is in striking contrast with the tropical Pacific, with a shallower thermocline and stronger warming to the north of equator. On the other hand, recent studies have reported that a strengthening of the AMOC is one of the reasons why the Northern Hemisphere has warmed rapidly and the Arctic sea ice has retreated drastically in recent years.<sup>94</sup> Yet, existing evidence attributes this to interdecadal variability that has weakened the AMOC lately.<sup>95,96</sup> Therefore, the future change of AMOC and its influence on regional climate remain inconclusive.

In the Southern Ocean, strong global subduction that forms polar mode water and deep convection generates downwelling and vertical mixing. These processes transport the GHG-induced heating from the surface to the deep ocean. As a result, warming at the surface and subsurface is reduced, except in the South Indian Ocean, where moderate warming is observed.<sup>91</sup>

In summary, surface ocean warming shows striking consistency in the Southern Hemisphere among various ocean basins, probably because the subduction of the Southern Ocean takes away surface heating and inhibits pronounced warming to occur in the subtropics. Equatorial regions show cross-basin dynamical consistency that may result from the similar air–sea coupling modes of the tropical oceans. In the Northern Hemisphere, however, distinctions emerge, for example, between the Atlantic and Pacific Oceans: subduction of the AMOC transports surface warming to the deep North Atlantic, symmetric with the subduction in the Southern Ocean. This leads to subsurface warming that is stronger in the Northern Hemisphere. In recent years, pronounced warming has occurred in the deep waters of the Atlantic and Southern Oceans, which has been suggested as evidence for enhanced deep ocean heat update during the so-called global warming hiatus.<sup>97</sup>

Investigation of global ocean warming has advanced our understanding of climate change considerably; however, nonuniformity of climate change between ocean basins is by no means understood clearly. The remaining challenges reflect the complexity of the scientific questions,

including detailed mechanisms of ocean circulation in different basins and their interactions, and data limitations of both short observational records and coarse horizontal sampling, especially for the deep ocean, as well as biases and inconsistencies between climate model simulations. In order to correctly understand the oceanic responses to climate change, the scientific community needs to further improve climate models, develop ocean exploration technology, conduct observational experiments, and analyze the observations (see below).

### **Influence on interannual variability**

The significant influence of regional climate change on the hydrological cycle mentioned above causes adjustments in atmospheric and oceanic circulation that affect interannual variability. The responses of ENSO, IOD, and Atlantic Niño to global warming are briefly reviewed in this section.

#### *ENSO response*

As the ENSO is the dominant mode of tropical interannual fluctuations, its response to increasing GHGs is of great interest, especially in terms of amplitude change in the past few decades and expectations for the future.<sup>25,47,98–102</sup> Observational studies reveal that ENSO amplitude has generally weakened during the past three decades, which has been accompanied by a strengthened zonal SST gradient as well as Walker circulation in the tropical Pacific. However, as for the future projections under global warming, the latest two IPCC Assessment Reports (i.e., AR4 and AR5) concluded that there are large discrepancies between climate models regarding ENSO amplitude change<sup>103,104</sup> despite a robust increase in the projected ENSO-driven rainfall variability.<sup>100,105</sup> Changes in ENSO amplitude result from competition among mechanisms amplifying and/or damping air–sea feedbacks involved in the ENSO cycle.<sup>25,59</sup> Hence, all of these mechanisms are potential sources of the intermodel uncertainty in the ENSO amplitude projection.

The sensitivity of atmospheric circulation and convective activity to local SST anomalies (SSTAs) is a crucial tropical air–sea interaction process in the Bjerknes feedback<sup>106,107</sup> and ENSO development in the eastern Pacific.<sup>108–110</sup> These adjustments in the Bjerknes feedback to global warming can be an important source of uncertainty for ENSO amplitude change among models.<sup>111</sup> Models

with an increased (decreased) sensitivity tend to amplify (weaken) El Niño through the Bjerknes feedback (Fig. 3). However, as the simulations of such sensitivity in current climate suffer from systematic bias,<sup>111</sup> models are unreliable in both predicting the present-day ENSO amplitude and projecting its change under global warming. Moreover, due to the nonlinearity of the SST–convection relationship,<sup>112–114</sup> the sensitivity is much less important for La Niña compared with El Niño.

The section above that describes the dynamical fundamentals of tropical climate change illustrated robust changes of the hydrological cycle over the tropical Pacific due to GHG warming, which establishes the background state for other adjustments. Specifically, a weakened atmospheric Walker circulation acts as a favorable condition for an El Niño–like mean SST change.<sup>17,115</sup> In CMIP5 models, this pattern exhibits an SST warming peak in the eastern equatorial Pacific that is stronger than in the western or in the tropical mean.<sup>116,117</sup> The associated, locally enhanced Hadley cells tend to destabilize the atmosphere at low levels and increase the atmospheric circulation sensitivity to the eastern Pacific SSTAs, and hence El Niño, through the Bjerknes feedback.<sup>55,111,117</sup>

Owing to the multiple sources of uncertainty involved in various ENSO feedbacks,<sup>25,110,118</sup> whether the amplitude of the full ENSO cycle will be enhanced or not cannot be answered definitively at present. Nevertheless, implications could be inferred when considering some robust mean-state changes in the hydrological cycle that are important to ENSO development. By applying a methodology called “emergent constraint” to the common biases in the historical simulations, mean SST and surface wind changes in the tropical Pacific are constrained to show a pattern of more enhanced warming in the eastern Pacific and weakened surface trade winds, which is closer to El Niño than the unconstrained ensemble mean.<sup>116,119,120</sup> These results imply a potential strengthening of El Niño under global warming through an enhanced sensitivity of atmospheric circulation response to SSTAs, consistent with previous studies.<sup>118,121</sup> However, other processes, including the oceanic feedbacks and their interactions with the mean state, may offset this strengthening<sup>122–124</sup> and complicate the El Niño amplitude change.

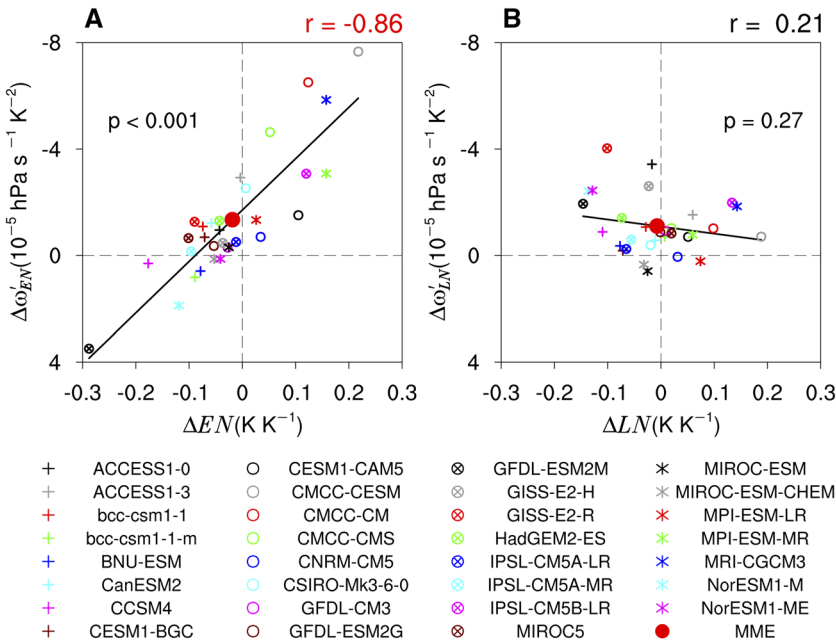


**Figure 3.** (A) Intermodel scatterplot between changes in the response of atmospheric circulation to SSTs over the Niño3 region for SSTA > 0 ( $\Delta\omega'_{EN}$ ) and the change of El Niño's amplitude ( $\Delta EN$ ). (B) Intermodel scatterplot between changes in the response of atmospheric circulation to SSTs over the Niño3 region for SSTA < 0 ( $\Delta\omega'_{LN}$ ) and the change of La Niña's amplitude ( $\Delta LN$ ). The sensitivity of atmospheric circulation to SSTs is defined by linearly regressing the interannual anomalies of 500-hPa vertical pressure velocity against the SSTs at each grid point. The amplitude of El Niño and La Niña is defined as the root mean square value of SSTs averaged over the Niño3 region for SSTA > 0 and SSTA < 0. Changes in both amplitude and circulation response are normalized by the mean SST change averaged between 60°S and 60°N. The solid line denotes the linear intermodel regression. The intermodel correlation coefficient is shown in the upper right corner of each panel, and the corresponding *P* value is shown in each panel. Red (black) numbers denote that the intermodel correlation is significant (insignificant) at the 99% confidence level, based on the Student's *t*-test.

As another background condition for ENSO development, ocean circulation and thermal structure can be affected by the weakening of the Walker circulation<sup>74</sup> and further influence ENSO characteristics. For instance, the flattening of the mean equatorial thermocline in response to the reduction of surface trade winds will potentially increase the occurrence of central over eastern Pacific El Niño.<sup>125</sup> Other responses of ENSO processes to hydrological cycle changes are still poorly understood, including ENSO onset, duration, termination, and transition between El Niño and La Niña. A reliable projection for the overall evolution of future ENSO properties requires climate models to reasonably reproduce all ENSO dynamical and thermodynamic processes, as well as their responses to global warming, including the influences of hydrological cycle changes and associated feedbacks.<sup>47</sup>

**IOD change**

The IOD is the dominant climate mode in the Indian Ocean on interannual timescales.<sup>126,127</sup> Through the IOD, the Indian Ocean plays an active role in climate, with pronounced global impacts.<sup>128</sup> An IOD index, defined as the difference of regional mean SSTs between the western equatorial Indian Ocean (within 50–70°E and 10°S–10°N) and the southeastern equatorial Indian Ocean (within 90–110°E and 10°S–0°), is often used as a proxy for the IOD in the context of climate change.

Low-frequency variations of the IOD are closely related to relative change of SSTs in the eastern and western poles of the Indian Ocean, which have both increased but at different rates. By examining monthly SST observations during 1880–2004, Ihara *et al.* showed that the eastern Indian Ocean warmed faster than the western basin before 1919, a condition favorable for negative IOD events.<sup>129</sup> The

period 1920–1949 appears as a transitional period, during which the temperature changes were relatively uniform zonally. SST over the western Indian Ocean has increased faster after 1950, and more positive IOD events have tended to occur.<sup>130,131</sup> Such trends are reproduced by the CMIP models. In the context of recent global warming, the Indian Ocean is subject to a relatively uniform SST increase, more like a basin mode.<sup>132</sup> As a result, the zonal surface atmospheric circulation through the Indian Ocean seems to be reduced (e.g., by MASC); however, the long-term variation of the IOD is much more complex due to the air–sea interactions. Cai *et al.* concluded that the number of positive IOD events has increased by 17% and more positive IOD events tend to occur in two or three consecutive years due to global warming in recent decades.<sup>133</sup> Furthermore, Cai *et al.* projected the frequency of extreme positive IOD events to increase by nearly a factor of three.<sup>100</sup> Such model simulations are quantitatively consistent with decadal variability of the IOD observed from coral records.<sup>134,135</sup> However, the overall frequency of the IOD does not change significantly, and the amplitude difference between the positive and the negative IOD events decreased in the 20th century.<sup>56</sup>

Fundamentally, SST trends can be jointly attributable to surface thermodynamics and ocean dynamics. Hydrological processes play an important role in the heat budget of the upper mixed layer. Du and Xie showed that the impacts of global warming on the Indian Ocean are amplified by water vapor feedback in the CMIP3 models.<sup>136</sup> Anomalies in low-level atmospheric circulation modify evaporation and the corresponding latent heat flux. Meanwhile, clouds are found to be the dominant source of uncertainty for the simulated IOD, consistent with uncertainties in the simulation of many other climate processes. Dynamically, the slow variation of the IOD is controlled by changes in thermocline depth, especially in the eastern tropical Indian Ocean.<sup>137</sup> A shallow (deep) thermocline over the eastern Indian Ocean is favorable for positive (negative) IOD events and weak (strong) IOD responses to the ENSO,<sup>138</sup> which has been confirmed by CMIP5 simulations.<sup>139</sup> A shoaling of the thermocline in the eastern tropical Indian Ocean strengthens the thermocline feedback, leading to an increase in the variance and a reduction of the negative skewness of the IOD.

The IOD has a close relation with the ENSO in the Pacific Ocean, for example, many IOD events coexist with ENSO events. However, their interactions are also subject to change, and their degree of independence is still uncertain.<sup>140</sup> Usually, a positive (negative) IOD event resembles a mirror image of El Niño (La Niña), although it was found that the decadal variability of the IOD and the ENSO was not well correlated.<sup>137</sup> Hence, an Indo-Pacific tripole mode was proposed,<sup>141</sup> which aimed to synthesize the IOD and the ENSO. The Walker circulation is the hinge between the IOD and the ENSO in the atmosphere. A weakened Walker circulation due to global warming<sup>22</sup> would lead to easterly wind anomalies in the lower troposphere over the tropical Indian Ocean. As a result, the equatorial thermocline would flatten and induce a thermal structure resembling the positive IOD, which is consistent with the El Niño-like response in the Pacific Ocean.

The Indonesian throughflow (ITF) is the bridge between the ENSO and the IOD in the ocean. Changes in ITF volume and its vertical stratification have pronounced impacts on the Indian Ocean, such as the thermocline dome over the southwestern basin.<sup>142</sup> In the context of global warming, the sea level rises in the Indian Ocean, which decreases the pressure gradient between the Pacific and the Indian Ocean. As a result, ITF and associated heat transport to the Indian Ocean tend to be reduced, while heat content increases in the Pacific Ocean.<sup>143</sup> Consistently, changes in ITF and heat exchange between the two oceans are found to be related to the recent hiatus of global warming.<sup>144</sup> In addition, the thermocline depth of ITF (in the Makassar Strait) also changed significantly after 2008/2009,<sup>145</sup> but the dynamics still require dedicated studies.

The ITF volume is basically controlled by the pressure gradient between the western Pacific and the eastern Indian Ocean.<sup>146</sup> During El Niño, the trade winds in the equatorial Pacific and the north equatorial ocean current become weaker. This reduces the Kuroshio current, which originates from the bifurcation of the northern equatorial current east of the Philippines. Consequently, more Pacific water enters the South China Sea (SCS) through the Luzon Strait. The SCS water can reach south of the Makassar Strait via the Karimata Strait as the SCS throughflow that is usually fresher than near the Maritime Continent. The resulting elevation in sea level works like a plug against the

major southward ITF mass transport through the Karimata Strait. The enhanced SCS throughflow<sup>147</sup> reinforces the freshwater plug in the south of the Makassar Strait.<sup>148</sup> Both the reduction of trade winds and the enhancement of the freshwater plug reduce the ITF.<sup>149</sup>

Variations in the ITF can modify the SST and ocean dynamics in the eastern Indian Ocean after it enters the basin between 10° and 15°S.<sup>150,151</sup> In addition, it can also have impacts on the western Indian Ocean, particularly in the thermocline dome region around the Seychelles.<sup>142,152</sup> The reduction in ITF is prone to inducing cool SSTAs over the eastern Indian Ocean, since the ITF transports warm and fresh water from the Pacific to the Indian Ocean. Therefore, an El Niño event may create a favorable environment for a positive IOD event. However, the ITF-induced ENSO influences on IOD and their robustness have not yet been clearly quantified.

It has also been proposed that the variability in the Indian Ocean may have feedbacks to the Pacific Ocean via equatorial planetary waves in the ocean.<sup>153</sup> Indeed, the IOD can leave footprints on the ENSO and such feedbacks may be active in response to global warming.<sup>128,154</sup> For example, simulations using a global ocean–atmosphere coupled model showed that extreme IOD events from 2006 to 2008 can significantly enhance El Niño and the forecast of its onset.<sup>155</sup> Nevertheless, such mechanisms are still under debate.

### *Atlantic Niño and meridional mode*

Attribution of the significant long-term trends going back several decades has been challenging for the tropical Atlantic. Since 1950, there has been significant warming of the basin, which is most pronounced in the eastern equatorial region during boreal summer.<sup>156</sup> The warming is associated with anomalous westerly near-surface winds in the central and eastern equatorial Atlantic, deepening of the thermocline, and increases in convection and precipitation in western equatorial Africa near the Gulf of Guinea. One possible cause of the anomalous warming in the eastern equatorial Atlantic is an increase in anthropogenic aerosol emissions in the Northern Hemisphere since 1950.<sup>156</sup> The aerosol effect has acted to cool the tropical North Atlantic and weaken the easterly trade winds in the equatorial Atlantic, deepening the thermocline and

increasing SST. Nevertheless, this may be reinforced by a phase shift of the AMO during 1955–1975.<sup>157</sup>

In contrast with the results of Tokinaga and Xie,<sup>156</sup> Servain *et al.*<sup>158</sup> showed an increasing trend in near-surface wind speed throughout the tropical Atlantic despite the strongest SST warming trends in the equatorial and intertropical convergence zone (ITCZ) regions of the Atlantic going back to the 1960s. That is, the increase in SST since the 1970s has likely been caused by changes in the AMOC or subtropical ocean cells. The results of Lübbecke *et al.*<sup>159</sup> support this view, showing that increased flow of warm Indian Ocean water through the Agulhas leakage and into the tropical Atlantic may have contributed to the observed warming trend. These previous studies illustrate the challenge of attributing trends in the tropical Atlantic to natural variability, anthropogenic aerosols, and GHGs. The differences in trends among observational data sets contribute to the difficulty.

Interannual variability in the tropical Atlantic projects strongly onto two modes: the Atlantic Niño and the Atlantic meridional mode (AMM). The Atlantic Niño is characterized by anomalous warming of SST in the eastern equatorial Atlantic that peaks in the boreal summer.<sup>160,161</sup> This mode is maintained in part through positive feedback between SST, equatorial zonal wind, and thermocline depth, that is, the Bjerknes feedback.<sup>162</sup> The AMM consists of an anomalous meridional gradient of SST centered near the equator that is associated with anomalous near-surface winds directed toward the warmer hemisphere and a displacement of the ITCZ over the warmer SST.<sup>163,164</sup> The AMM tends to peak in the boreal spring<sup>165,166</sup> and is enhanced by the positive wind–evaporation–SST feedback.<sup>106,167</sup>

Through changes in air–sea heat fluxes, atmospheric circulation, and convection, the Atlantic Niño and AMM affect rainfall over the surrounding continents, sometimes leading to severe droughts or floods.<sup>168–172</sup> The AMM additionally affects North Atlantic hurricane activity,<sup>173</sup> and, more generally, tropical Atlantic variability modulates the ENSO and the Asian monsoon. Warming associated with an Atlantic Niño causes anomalous subsidence over the rest of the tropics, favoring a La Niña state in the equatorial Pacific and affecting ENSO prediction,<sup>174,175</sup> and leading to a weakening of the Asian summer monsoon.<sup>176</sup> Anomalous warming

in the tropical North Atlantic associated with the AMM has also been shown to interact with the ENSO.<sup>177–179</sup>

Under global warming, the deepened thermocline in the central and eastern equatorial Atlantic makes the SST less responsive to wind and thermocline changes, which will weaken the Atlantic Niño variability and decrease the magnitude of interannual rainfall variations in western Africa. However, projections of changes in the Atlantic Niño and AMM under global warming are difficult due to large systematic biases in coupled model simulations of the tropical climate.<sup>180,181</sup> One way to alleviate this difficulty is to force an atmospheric model with historical and future projections of SST. Using this technique, Mohino and Losada<sup>182</sup> found that climate change will lead to an eastward shift of rainfall anomalies in the eastern Atlantic associated with the Atlantic Niño and a weakening of negative Atlantic Niño-induced rainfall anomalies from the Asian summer monsoon. However, future changes in Atlantic Niño and AMM characteristics, such as frequency and intensity, and their potential impacts on regional and global climate remain unclear. An important ongoing challenge is reducing biases present in many coupled climate models that have not been corrected much during the past two decades.<sup>181</sup> It is important to correct these biases in order to generate useful projections for tropical Atlantic variability under various climate change scenarios.

## Impact on monsoons

Monsoon climates display strong seasonality, characterized by a distinct wet summer and dry winter, usually with opposite wind directions. Across the globe, areas affected by monsoon account for approximately 20% of the Earth's surface and monsoon precipitation accounts for 30.8% of total precipitation.<sup>183</sup> Moreover, more than two-thirds of the human population lives in monsoon regions, where the variability of monsoon precipitation exerts profound socioeconomic influences. This section summarizes changes in the global monsoon (GM) system and then downscales to the Asian and South American regions and discusses monsoon modulations by the ENSO. It is noteworthy that the African monsoon precipitation tends to increase in a warmer climate, but the extent is not as remarkable as that of the South Asia monsoon.<sup>57</sup>

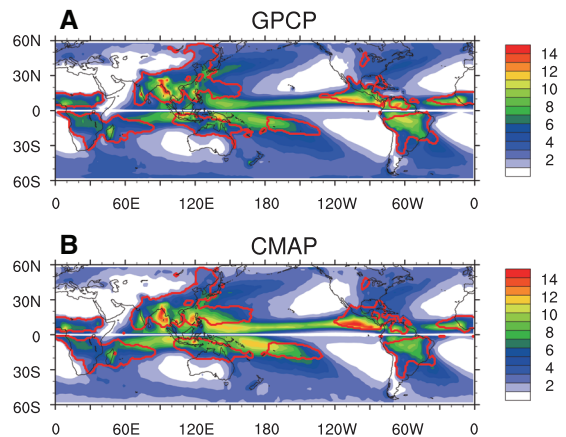


**Figure 4.** The climatological (1980–2005) monsoon rainfall (color shading; mm/day) and monsoon areas (red lines) in the results of GPCP (A) and CMAP (B). The monsoon rainfall is the local summer (May–September/November–March in the Northern/Southern Hemisphere) mean. This figure is adapted from Ref. 186.

## The global monsoon system

The concept of the GM was proposed by Trenberth *et al.*<sup>184</sup> and Wang and Ding.<sup>183</sup> Here, the wet (dry) season is defined as May–September (November–March) in the Northern Hemisphere, and opposite in the other hemisphere. The GM is quantified by precipitation, an essential feature with areas in which the wet season rainfall accounts for no less than 55% of the annual rainfall (e.g., Refs. 183 and 185). The monsoon rainfall and areas<sup>186</sup> are displayed in Figure 4. The GM variation can be recognized as the first leading mode in a multivariate empirical orthogonal function performed for the annual cycle of precipitation/850 hPa winds, reflecting the impact of antisymmetric solar forcing with a 1- to 2-month delay in atmospheric circulation. In a warming climate, the following changes of the GM have been predicted.<sup>187,188</sup>

**GM areas expand in projections with climate models.** RCP4.5 modes project a 1–10% area increase, with the 50th percentile at 5.4%.<sup>187</sup> The ensemble mean increase is 3–5%, equivalent to 1–2% K<sup>-1</sup> of global mean surface warming.<sup>57,185</sup> The expansion mainly occurs over the central to eastern tropical Pacific, southern Indian Ocean and eastern Asia,<sup>187</sup> with twice as much over the ocean as over land.<sup>185</sup> The GM wet season will likely increase in duration. Over the globe, as the GM withdrawal

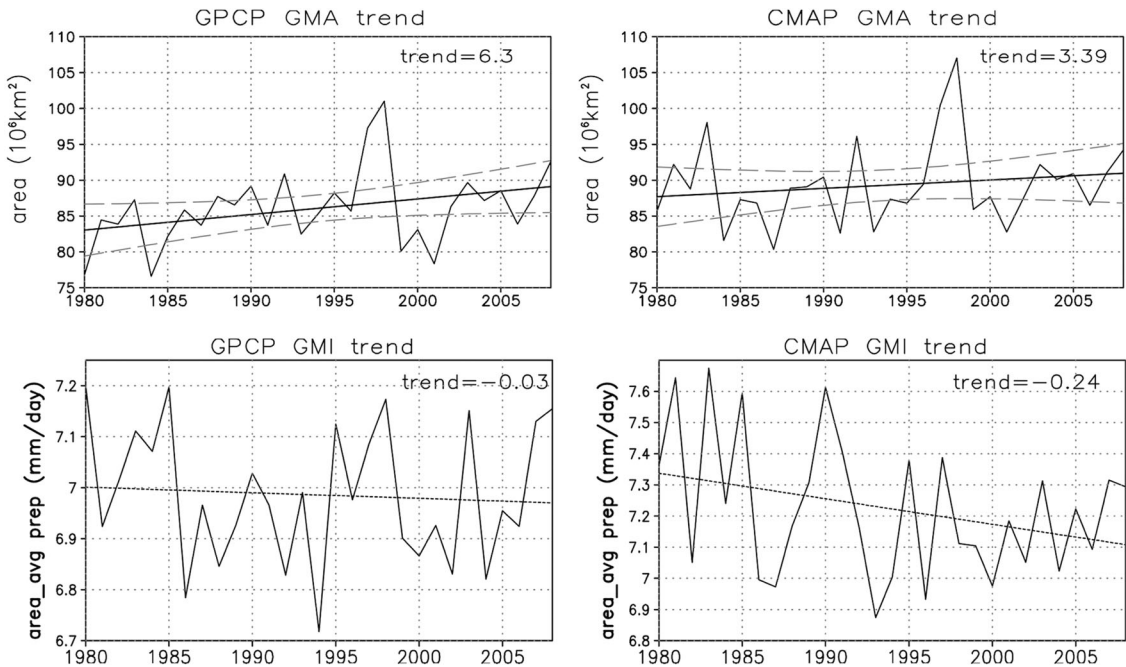


**Figure 5.** Time series of the global monsoon (upper) area (GMA;  $10^6 \text{ km}^2$ ) and (lower) intensity (GMI; mm/day) calculated based on the GPCP (left) and CMAP (right) data sets for the period of 1979–2008. The linear trend of each time series is presented by a dashed line, with the value of the change during this 27-year period shown in each panel. This figure is adapted from Ref. 189.

dates delay, the onset dates will either advance or change little.<sup>187</sup> Especially, the monsoon onset will advance in the Northern Hemisphere, which may be largely attributed to the overall precipitation increase in May.<sup>57</sup>

**GM precipitation increases.** In response to global warming, the atmospheric circulation tends to slow down, reducing GM convection and precipitation as a dynamical effect. However, atmospheric moisture increases as climate warms and overwhelms the dynamical effect of the wet-get-wetter mechanism (see above), leading to enhanced GM precipitation as a thermodynamic effect.<sup>188</sup> Consistently, evaporation increases due to a larger difference between surface-air specific humidity and the saturated one at SST.<sup>185</sup> The CMIP5 ensemble mean GM precipitation increase is 5.7%, or 3–4%  $\text{K}^{-1}$  of global mean surface warming. Similar to the area expansion, the increasing rate of GM precipitation over the ocean is also twice that over the land.<sup>185</sup>

**The mean intensity of GM precipitation (precipitation per unit area) increases.** In response to

$\text{CO}_2$  forcing, the upper troposphere warms more than the lower troposphere, leading to a more stable atmosphere.<sup>77</sup> Consequently, the frequency of precipitation events decreases, and the average intensity of precipitation is stronger as more moisture is available in a warmer atmosphere.<sup>187</sup> Monsoon precipitation reacts distinctly between the hemispheres. The monsoon rainfall is projected to increase 3.1%  $\text{K}^{-1}$  of global mean surface warming in the Northern Hemisphere but slightly decrease in the Southern Hemisphere.<sup>57</sup> Among the GMs, the Asian monsoon is unique in both formation and response to a warmer climate, which will be discussed in the following section.

In order to compare with the above model projected changes, we illustrate recently observed trends in Figure 5.<sup>189</sup> During the past several decades, the GM area and total precipitation increases similarly with those in future projections; however, the GM intensity decreases, opposing the future changes. This uncertainty in the observations might result from internal variability instead of global warming.

### *Asian monsoon system*

The Tibetan Plateau plays a crucial role in the formation and distribution of the Asian monsoon. Model simulations indicate that in boreal summer, the heating and insulating effect of the Tibetan Plateau forms a huge heat source in South Asia.<sup>190,191</sup> This enhances the southerly/southwesterly winds over East Asia,<sup>192</sup> transports moisture further northward, and extends the edge of the Asian monsoon to the northernmost position among all monsoon domains.<sup>193</sup>

In a warmer climate, the Asian monsoon precipitation will likely increase much more than that of any other monsoon system in both the average and the extreme, though there is great uncertainty in these projections caused in part by aerosols.<sup>187,188,194</sup> Consistent with the GM, the thermodynamic effect in the Asian monsoon overcomes the dynamical effect to dominate the rainfall change.<sup>188,195</sup> Moreover, the decrease in ascending motion of the Asian monsoon in response to global warming is partially offset by the increase associated with the enhanced land–sea thermal contrast.<sup>194,196</sup> This leaves a small residual weakening in upward motion that is insignificant compared with other monsoons, giving rise to the wet-get-wetter effect. In addition, a large increase in surface evaporation contributes to a pronounced enhancement of Asian monsoon precipitation.<sup>188</sup>

Moisture transport associated with the Asian monsoon circulation is generally enhanced under global warming. More precipitation is associated with increased boreal summer latent heating over the Tibetan Plateau and the strengthening of the low-level East Asia monsoonal flow and its moisture transport.<sup>197</sup> By contrast, the monsoon circulation in South Asia tends to decrease by 15%, but the associated moisture transport is strengthened due to atmospheric warming and moistening.<sup>198</sup>

Physically, the rise of GHG concentrations changes regional climate mainly through direct radiative and SST-mediated processes, which exert different dynamical and thermodynamic effects on the Asian monsoon. Specifically, the direct radiative effect leads to an intensified land–sea thermal contrast as well as convergence over Asia, contributing to an increase in Asian monsoon rainfall. The SST-mediated effect warms and moistens the atmosphere over Asia through ocean-to-land advection, intensifying the monsoon rainfall. However, this

SST effect also includes a reduction of the land–sea thermal contrast over Asia, leading to divergence and weakening rainfall over Asia. Overall, the radiative effect includes a positive dynamical component and nonsignificant thermodynamic component, but the SST mediates a negative dynamical effect and stronger positive thermodynamic effect.<sup>194,199</sup>

The aforementioned studies on the Asian monsoon circulation and rainfall change in response to global warming are largely based on the analysis of general circulation model results, for which differences in model physics often induce large uncertainties in climate projections. Nonetheless, since most models consistently project an increase in atmospheric moisture, uncertainties in the thermodynamic effect are relatively small. By contrast, changes in ascent or convergence are strongly affected by patterns of SST warming that show great diversity among models. Thus, the uncertainty arising from the dynamical effect is relatively large.<sup>199</sup>

### *South American hydrology*

Analyses of several observational data sets have shown robust increase in surface air temperature over South America during the past few decades. Central Brazil is the region leading the annual mean warming over much of the continent.<sup>200</sup> By contrast, annual precipitation has a significant positive trend in only one of the adopted data sets,<sup>200</sup> because rainfall change varies much in space, with a robust increase in only one region, roughly encompassing the southern part of La Plata Basin (southern Brazil, Uruguay, and northeastern Argentina). The historical CMIP5 simulations do not capture this feature. It is, therefore, difficult to reach firm conclusions on precipitation trends in South America due to considerable geographical variations and the strong influence of SST variability.<sup>201</sup>

Barkhordarian *et al.*<sup>202</sup> examined seasonal trends in the observed warming during the period 1983–2003 in daily maximum and minimum near surface air temperatures ( $T_{\max}$  and  $T_{\min}$ , respectively) over South America. This was done by applying a detection and attribution (D&A) methodology, in which natural variability and forced trends are estimated from long-term simulations in CMIP5 models with different scenarios of GHG and aerosol concentrations. The detection component of D&A revealed that in the wet seasons the natural modes of variability explain a substantial portion of  $T_{\min}$

and  $T_{\max}$  variability. However, the warming trend during the dry seasons (June–August, September–November (SON)) is well beyond the range of natural (internal) variability influenced by the ENSO, the Pacific decadal oscillation (PDO), and the SAM. The attribution component of D&A revealed that the observed anthropogenic warming in SON is up to 0.6 K per decade over central Brazil and northern Argentina, which is not reproduced by any of the global and regional climate change projections. It also showed that anthropogenic aerosols have a detectable influence in SON and that the indirect effect of aerosols on cloud lifetime is more compatible with the observed record. An increasing trend in the observed incoming solar radiation over northern South America in SON was found to be larger than expected from natural (internal) variability alone.

In a follow-up study on the dry season over tropical South America, Barkhordarian *et al.*<sup>203</sup> addressed the observed drying during 1983–2012 over southern Amazonia and central Brazil. Their analysis captured negative trends in precipitation during the past decades that exceed the estimated range of natural variability in the climate system. Moreover, a bivariate (two-dimensional) attribution analysis pointed to elevated GHG levels and land-use change as the key causes of the drying. Thus, it was suggested that the recent trend to a drier dry season over northern South America will intensify in the course of unfolding anthropogenic climate change. Such change could have profound societal and ecological impacts on the region. In particular, Barkhordarian *et al.*<sup>204</sup> showed an increasing trend over tropical South America in vapor pressure deficit, a key driver of plant transpiration and photosynthesis. Drier and longer dry seasons can have significant influences on the ecosystem microclimate and the hydrological cycle in tropical South America.

### *Monsoon modulations by the ENSO*

The monsoon systems vary markedly at seasonal to orbital timescales, and the major processes that drive their variations are distinct across the timescales.<sup>205–207</sup> On the interannual timescale, the ENSO is the dominant factor that modulates the monsoon pattern and variability.<sup>208,209</sup> During El Niño, droughts often occur in monsoon regions like South Asia, Australia, and West Africa,

while wet conditions prevail in monsoon regions like East Asia, East Africa, and southwest North America.<sup>209,210</sup> In general, these impacts reverse during a La Niña event.

Here, we illustrate some examples in more detail. Modern observational records indicate that the ENSO influence on the South Asian summer monsoon (SASM) was significant over most of the 20th century, but it has weakened substantially since the late 1970s.<sup>211</sup> By contrast, the overall coupling between the ENSO and the western North Pacific, East Asian, and Indonesian monsoons have strengthened since the late 1970s, overriding the concurrent weakening of the ENSO–SASM anticorrelation.<sup>212,213</sup> ENSO effects are also primarily responsible for the interannual variability of South American monsoon precipitation. The warm (cold) phase of ENSO is generally associated with below (above) average precipitation in northern South America during the warm season and with enhanced (reduced) precipitation in southeastern South America.

However, the ENSO influence on the monsoon climate is largely through atmospheric teleconnections and is nonstationary over time. For instance, El Niño (La Niña) events in the cold (warm) AMO phase tend to be stronger than in the warm (cold) AMO phase.<sup>210,214,215</sup> Overall, observational records collectively indicate that the strength of the ENSO influence on the GM climate has waxed and waned over time, although regional manifestations have varied and its robustness can hardly be scrutinized due to the shortness of the observations.<sup>216</sup> Thus, high-resolution paleoclimate records have been employed to provide a long-term perspective to the examination of the ENSO–monsoon modulations. Similar to observational records, decadal to centennial variations in the strength of ENSO teleconnections on precipitation or moisture have been observed as robust features in all major monsoon regions during the past few centuries to millennia.<sup>205,217–219</sup>

In addition to the paleoclimate records, ensemble runs of models show tremendous natural variability despite the fact that they cannot simulate ENSO very accurately. Numerous studies have been conducted to understand the factors that drive the modulations of the ENSO–monsoon relationship. A number of major processes have been identified, including a shift between the eastern Pacific

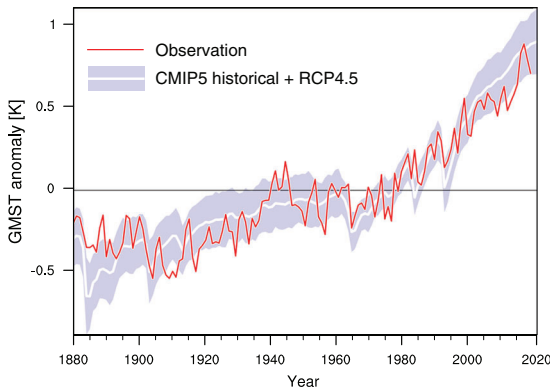


**Figure 6.** Global mean surface temperature (GMST) anomalies since 1880, from observations and CMIP5 historical simulations with the RCP4.5 scenario. The average of observations (red curve) is derived from NOAA GlobalTemp v5,<sup>228</sup> GISTEMP v4,<sup>229</sup> and HadCRUT 4.6.0.0.<sup>230</sup> The CMIP5 multi-model ensemble mean (white curve) and  $\pm$  unit ensemble standard deviation (blue shading) are calculated from 110 members of 37 models. All GMST anomalies for observations and CMIP5 models are relative to their 1961–1990 averages.

and central Pacific El Niño,<sup>220,221</sup> disturbance due to regional atmosphere–ocean interactions,<sup>213,222</sup> variations in the Pacific and/or Atlantic mean state related to the PDO and/or the aforementioned AMO,<sup>223,224</sup> and the long-term changes in ENSO activity.<sup>219,225</sup>

Nonetheless, substantial future progress is necessary to pinpoint the nature of ENSO–monsoon modulations and the driving mechanisms of their dynamical relationships on different timescales. Improvements in climate models are crucial in this regard, as currently they have limited success in simulating the ENSO–monsoon modulations.<sup>218,226,227</sup>

### Interdecadal variability and global warming

Global mean surface temperature (GMST) increased by more than 1 K during the past century, but this warming was not monotonic. Observations<sup>228–230</sup> and simulations shown in Figure 6 indicates substantial interdecadal fluctuations of GMST, with acceleration and deceleration of warming, such as the early 20th century fast warming and the global warming hiatus in the 2000s. The interdecadal modulation is so important that the CMIP6 (see below) exclusively includes a set of pacemaker experiments<sup>58</sup> to examine it with a large multimodel ensemble in the aforementioned

Decadal Climate Prediction Project (DCPP). This section reviews the current understanding of how GMST has been modulated by internally generated interdecadal variability.

#### Early 20th century warming

While warming since the 1960s is largely attributed to anthropogenic GHG forcing, the comparable early 20th century warming (ETCW) has long been mysterious.<sup>231</sup> During this period, GHG radiative forcing was three to four times weaker than at present,<sup>232</sup> and the reduction in observed sea ice extent was small.<sup>233</sup> These differences suggest that mechanisms other than GHG forcing played key roles in ETCW. Applying an optimal detection/attribution methodology to observations and simulations, Shiogama *et al.*<sup>234</sup> found that the recovery from large volcanic activity and increase in solar irradiance contributed to ETCW, consistent with Refs. 235 and 236. On the other hand, Andronova and Schlesinger<sup>237</sup> and Ring *et al.*<sup>238</sup> indicated that the ETCW can be primarily attributed to internal variability, with GHG forcing only a secondary factor. The ensemble mean of CMIP5 all-forcing simulations explains only 20–40% of the observed GMST increase from 1910 to the 1940s (Fig. 6), reflecting the importance of internal variability.

The Arctic is one of the most sensitive regions of ETCW,<sup>231</sup> with a 60°–90°N mean surface warming of 1.5 K from 1910 to the 1940s,<sup>239</sup> compared with the contemporary GMST increase of 0.2–0.3 K. The positive albedo feedback cannot explain the early Arctic warming because observations show an insignificant reduction in sea ice extent. On the other hand, recent studies suggest that the interdecadal variability in the Pacific and Atlantic played a major role in the pronounced Arctic warming in the early 20th century. By forcing an atmosphere-only model with an improved SST product, Tokinaga *et al.*<sup>240</sup> mainly attributed the ETCW over the entire Arctic to concurrent negative-to-positive phase shifts of the IPO and the AMO in the mid-1920s, by intensifying warm advection of near-surface air into the North American and Eurasian Arctic regions. Svendsen *et al.*<sup>241</sup> reported similar advection enhancement due to a deepening of the Aleutian low associated with the negative-to-positive phase shift of the IPO. In their model simulations, the Aleutian low deepening further weakens the polar vortex, leading to

subsidence-induced adiabatic heating at the Arctic surface. Both studies highlight the importance of internally generated interdecadal variabilities for ETCW and the need for a reliable reconstruction of their historical evolution.

### *Global warming hiatus in the late 1990s–2000s*

Despite a continuous increase in well-mixed GHGs, the GMST rise slowed down unexpectedly in the late 1990s–2000s. This slowdown is commonly known as the global warming hiatus.<sup>20,242–248</sup> The global mean SST increased at  $0.14 \pm 0.06$  K per decade<sup>9</sup> during 1993–2012, which is less than half of the  $0.30 \pm 0.02$  K per decade projected by the CMIP5 simulations (95% confidence intervals). This weaker trend results from a relatively flat temperature evolution after 1998; hence, the inconsistency is more striking for the past 15 years (1998–2012) between the actual warming of  $0.05 \pm 0.08$  K per decade and the predicted change of  $0.21 \pm 0.03$  K per decade. The strongest hiatus signals are found in the tropics because omission of tropospheric and surface observations in the polar regions does not significantly affect the global mean.<sup>249</sup>

As the hiatus has received considerable attention from both the scientific community and general public, a number of recent studies have investigated its mechanisms and influences on ocean circulation. For instance, this phenomenon is found to be a characteristic of the near-surface temperature but does not represent a slowdown of the whole climate system warming, implying the redistribution of heat into the deeper ocean.<sup>97,250,251</sup> Another culprit could be volcano eruptions that cool the climate through reducing shortwave radiation.<sup>246</sup> Here, we elaborate on the internal variability,<sup>20,58,243,247,252</sup> with interbasin effects.<sup>21,253,254</sup>

A La Niña-like trend pattern due to a positive-to-negative shift of the IPO has been suggested as the major contributor to the hiatus.<sup>20</sup> While this SST change largely originates from natural interdecadal climate variability, the anthropogenic aerosol forcing also partly contributed to the La Niña-like trend pattern during the hiatus period.<sup>255,256</sup> A novel modeling method was used to identify recent cooling in the eastern equatorial Pacific as the key to reconciling climate simula-

tions and observations. In addition to radiative forcing, global temperature change was simulated by prescribing the observed history of SST over the central to eastern tropical Pacific.<sup>20</sup> Although limited to only 8.2% of the global surface, this SST prescription enabled a successful reproduction of the annual mean global temperature, with a correlation coefficient of 0.97 for 1970–2012. Moreover, the simulation captured the major seasonal and regional characteristics of the hiatus, including the intensified Walker circulation,<sup>243</sup> winter cooling in northwestern North America, and prolonged drought in the southern United States. Kosaka and Xie<sup>58</sup> also found similar hiatus events in 1896–1910 and 1962–1976, coincident with La Niña-like SST changes. Meehl *et al.*<sup>252</sup> linked these hiatus decades with the negative phases of the IPO, which internally generates cooling in the tropical Pacific to offset the externally forced global warming.

During the hiatus period, the AMO shifted from a negative to a positive phase, a change opposite to the IPO. Several studies have highlighted the interbasin impact from the tropical Atlantic instead of the stand-alone influence in the Pacific. McGregor *et al.*<sup>21</sup> found that the La Niña-like variability has been driven mainly by the recent pronounced Atlantic SST warming and the corresponding trans-basin redistribution of atmospheric pressure, which is associated with North American rainfall trends and western Pacific sea-level rise. Similarly, Li *et al.*<sup>253</sup> concluded that the tropical Atlantic played a key role in initiating the tropics-wide teleconnection during the past three decades. A tropical Atlantic pacemaker experiment indicated that the Atlantic-induced anomalies contributed nearly 55–75% of the tropical SST and circulation variations during the satellite era. Applying a semiempirical approach, Steinman *et al.*<sup>254</sup> combined climate observations and model simulations to estimate multidecadal variability in the Atlantic and Pacific. The study found that interdecadal signals explain a large proportion of the recent “false pause” in global warming, with competition between a modest positive peak in the Atlantic and a substantially negative phase in the Pacific. Although similar decadal hiatus events may occur in the future, the long-term warming trend is expected to continue as GHG concentrations increase.<sup>247</sup>

Both IPO- and AMO-induced SST changes have a significant influence on regional patterns of

precipitation change during the satellite era.<sup>209,257,258</sup> The La Niña-like SST changes enhanced (suppressed) deep convection over the tropical western (the equatorial central to eastern) Pacific, while the positive AMO changes increased precipitation over the subtropical North Atlantic. These SST precipitation changes are characterized by warmer-get-wetter patterns, which played a primary role in regional patterns of precipitation trends during the satellite era.

A recent study<sup>259</sup> has shown that surface-drifting and moored buoy measurements have a cold bias of 0.12 K compared with ship-based observations, and the global coverage of buoys has increased by up to 15% in recent decades. Because the global SST data sets mostly employ both types of observing systems, this will cause a cold bias in the trend estimation for the global mean SST. After this cold bias of the buoy data is corrected, it is possible to reject the existence of the hiatus. Another study<sup>260</sup> used a more rigorous and comprehensive statistical analysis rather than a simple trend calculation, which leads to an increase in the significance of the positive warming trend after the year 2000. However, by carefully examining the results of Ref. 259, the present study found that the global surface temperature had a rather weak trend during 1950–1970, and then increased significantly during 1971–2000, which apparently shows a warming trend stronger than 2001–2014. The test of the significance of warming during the early 21st century depends strongly on the period selected in the 20th century. Therefore, it is possible that the corrected data set still shows evidence for a smaller increasing linear trend over the past 15 years than over the past 45 years, that is, a pacemaker effect of interdecadal variability on presumably continuous global warming.

## Discussion and outlook

### *Previous progress*

Global warming is often defined using simple metrics, such as the change in Earth's mean surface temperature, because climate change impacts are generally thought to be in scale with global mean temperature. However, ultimately what are most meaningful from societal and decision-making standpoints are projections of how climate change will affect specific regions in terms of rainfall, extreme weather events, sea-level rise, etc. Advancements in climate modeling and theory and

sustained global observing systems have improved our understanding of regional climate change and enhanced our capability to predict their future changes.

With a globally uniform increase in GHG concentrations, robust regional differences in surface warming will occur. The regional response of ocean surface temperature to global warming depends on factors, such as preexisting basin-scale atmospheric and oceanic circulations, as well as SST patterns. In the tropics, these warming patterns drive changes in surface wind, atmospheric convection, and rainfall that interact with global-scale changes in air temperature, humidity, and three-dimensional atmospheric circulation.

The ENSO dominates the year-to-year variability of the tropical climate. Under continuing global warming, the ENSO is predicted to change, with potential effects on its predictability and global impacts. There are indications that El Niño events may become stronger under global warming, although the changes in the overall nature of the ENSO cycle, including the prevalence of eastern Pacific versus central Pacific events, remain unclear.

The Atlantic analog of El Niño, termed the Atlantic Niño, affects atmospheric circulation in the Atlantic and equatorial Pacific. Observations showed a long-term warming trend and associated deepening of the thermocline in the eastern equatorial Atlantic, which has weakened negative Atlantic Niño variability and decreased its associated rainfall variability in western Africa. Future changes in Atlantic Niño characteristics and their interbasin impacts remain unclear.

The Indian Ocean has a dipole mode nearly resembling a mirror image of ENSO, namely the IOD. The IOD and ENSO are connected by the Walker circulation in the atmosphere and bridged by the ITF in the ocean. A global warming-induced shoaling of thermocline in the eastern tropical Indian Ocean would strengthen the IOD activity. Positive IOD events, especially the extreme ones, are projected to increase based on model simulations. However, the overall frequency may not change significantly.

Monsoons provide rainfall to sustain large portion of the human population, underscoring the importance of understanding their interactions with the ENSO and long-term changes. Despite a future slowdown of the tropics-wide atmospheric

circulation, GM rainfall is expected to increase and the monsoon season is projected to lengthen. However, there are notable differences among monsoon systems, in which rainfall depends on conditions such as land–sea heating contrast and orography.

GMST, the most commonly used metric of climate change, has not risen at a uniform rate, but has experienced prolonged periods of reduced or enhanced warming due to natural variability. Most recently, there was a decade-long period of warming pause during the late 1990s–2000s. This warming hiatus has been linked to a natural decadal cycle in the Pacific Ocean that may have been enhanced by warming in the Atlantic Ocean. It is important to understand the causes of these natural changes in order to improve interdecadal climate predictions and to help improve longer term projections into the future.

### *Outlooks based on CMIP6 projections*

Along with the evolution of CMIP1–5, the research community has recognized a number of great challenges as the scientific backdrop for the organization and design of experiments for phase 6 of the CMIP.<sup>85</sup> The mandatory items in CMIP6 are Diagnosis, Evaluation, and Characterization of Klima (DECK) experiments (*klima* is “climate” in German) and historical simulations (1850–2014). The DECK experiments consist of Atmospheric Model Intercomparison Project (AMIP), preindustrial control (piControl), 1% per year CO<sub>2</sub> increase (1pctCO<sub>2</sub>), and abrupt CO<sub>2</sub> quadrupling (abrupt-4 × CO<sub>2</sub>) simulations.

CMIP6 endorses 23 additional MIPs, including not only previously existing projects like ScenarioMIP (advanced representative concentration pathways (RCPs)), but also novel projects such as AerChemMIP (aerosols and chemistry), GeoMIP (geoengineering), and HighResMIP (high resolution). Simulations in the endorsed MIPs are grouped into tiers to ensure community engagement. Only the Tier 1 experiments are overseen by the CMIP Panel, while additional experiments proposed by the MIPs are assigned to Tiers 2 and 3. Tier 1 experiments have the highest priority, demanding at least eight modeling groups to perform runs and provide all requested diagnostics for answering at least one of the MIP’s leading science questions.

The present study addresses several great challenges regarding hydrological cycle changes and

their impacts on climate variability, yet there remain issues concerning the improvement in understanding, predictability, and projection into the future. Examples of these challenges are changes in clouds, circulation and climate sensitivity, climate extremes, regional sea-level rise, and water availability. Here, we discuss some promising advantages of the new projections in resolving those related to this review, including but not limited to the following future research directions.

**Regional climate change in the tropics.** The new CMIP6 output (Fig. 7) resembles CMIP5 results (Fig. 1) in patterns but is enhanced in magnitudes, especially for the historical runs. Hence, strong uncertainty still remains, probably originating from the lack of understanding in pattern formation processes, including ocean heat content (mixed layer depth), ocean–atmosphere feedbacks, convection, and energy and moisture transports. The interactions with the very complex and uncertain role of cloud feedbacks are still one of the greatest challenges. CMIP6 targets them with new experiments such as the ScenarioMIP, Flux-Anomaly-Forced Model Intercomparison Project (FAFMIP), and CFMIP described below.

The ScenarioMIP adopts updated RCPs based on the Shared Socioeconomic Pathways (SSPs), plus some gap scenarios uncovered by the RCPs. SSP1–5 range from a societal development with greatest sustainability to one fully dependent on fossil fuel. Emissions and land-use scenarios are then generated with integrated assessment models based on these configurations. Each SSP $x$ – $y$  forcing pathway combination represents an integrated scenario of future climate and societal change, where  $x$  represents the SSP and  $y$  is the RCP. The Tier 1 experiments include SSP1–2.6, SSP2–4.5, SSP3–7.0, and SSP5–8.5.

The FAFMIP is designed to address uncertainties in projections of sea-level rise, including its global mean due to thermal expansion induced by ocean heat uptake and its geographical patterns due to ocean density and circulation change in response to CO<sub>2</sub> forcing.<sup>261</sup> In FAFMIP, surface fluxes such as momentum, heat, and freshwater are prescribed with corresponding perturbations from 1pctCO<sub>2</sub> experiments to piControl runs. This experimental setup might also be utilized to diagnose SST pattern change through the surface heat flux budget.

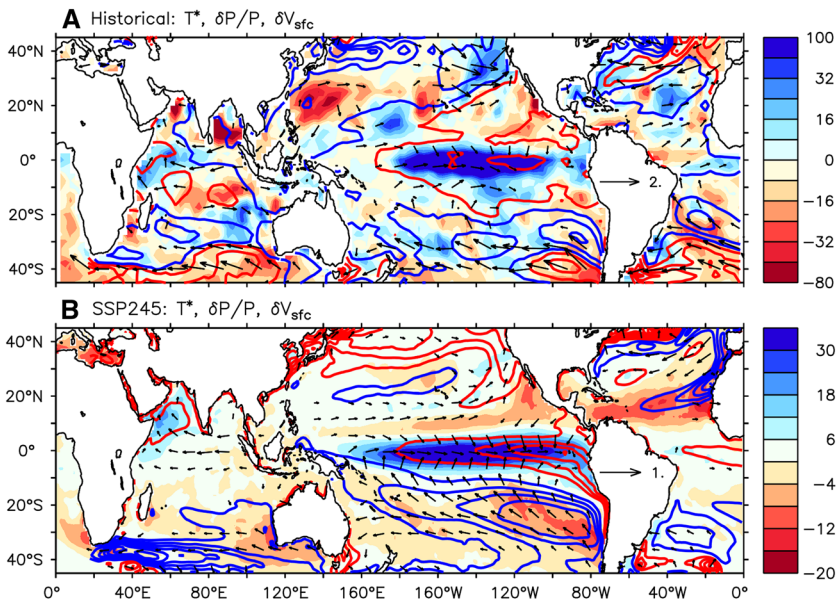


**Figure 7.** Same as Figure 1 but for CMIP6 models with the SSP2–4.5 scenario (2091–2100 minus 2015–2024) updating the RCP4.5.

Besides the DECK experiments, the Cloud Feedback Model Intercomparison Project (CFMIP, phase 3) has been further developed from CMIP5 to reinforce the understanding of cloud–climate feedback mechanisms and to improve the evaluation of clouds and cloud feedbacks in climate models. Besides the CFMIP2 experiments (AMIP, AMIP-p4K (-m4K), AMIP-4  $\times$  CO<sub>2</sub>, and AMIP-future4K), Tier 1 has added several corresponding aquaplanet simulations, and Tier 2 is very complicated to test multiple mechanisms of land rainfall change. The CFMIP3 experiments will be useful to test the SST pattern effect on cloud change and feedbacks, which has been attempted in recent studies on water vapor<sup>60</sup> and clouds.<sup>262</sup>

**Interannual and interdecadal variabilities.** The endorsed MIPs plus the DECK experiments favor the understanding of various climate modes. For the ENSO, the Atlantic Niño, and the IOD, their magnitudes, frequencies of occurrence, spatial patterns, interbasin connections, and impacts on the hydrological cycle are the major targets to address. For example, considering cloud feedback as the leading source of uncertainty in the SST warming,<sup>263</sup> the CFMIP and HighResMIP could be invoked to test its effect on ENSO amplitude change. The DCP, continued from CMIP5, is useful for climate modes that feature interdecadal variability, for example, its impacts on the global surface temperature rise and interactions with ocean circulation.

**Monsoons.** The sensitivity of monsoons to changes in surface temperature, land–sea thermal contrast, atmospheric circulation, and aerosols is still poorly understood. CMIP6 has added the Global Monsoons Modeling Intercomparison Project (GMMIP), with specific experiments and sensitivity tests to serve monsoon studies and simulations for multiple timescales from orographical maintenance, interannual variability, to historical and future evolutions. The experimental setup in GMMIP includes:

Tier 1: Extended AMIP run over 1870–2013.

Tier 2: Pacemaker runs in 20th century (to understand IPO and AMO effects).

Tier 3: Topography change experiments (Tibetan Plateau, Africa, America).

These experiments may help resolve some of the open questions described in the section above on monsoons.

Continued progress will depend on sustained international commitments to advances in

process-level understanding, regional climate modeling, and global climate observations. The CMIP6 efforts are directly addressing these with a new generation of climate models. We foresee a strengthened development of climate change science through the combination of these model outputs with innovative observational methodologies, for example, for clouds and ocean mixing.

## Acknowledgments

We acknowledge various modeling groups for producing and providing their output, the Program for Climate Model Diagnostics and Intercomparison for collecting and archiving the CMIP3, CMIP5, and CMIP6 multi-model data, the WCRP's Working Group on Coupled Modeling for organizing the analysis activity, and the Office of Science, the U.S. Department of Energy for supporting these data sets in partnership with the Global Organization for Earth System Science Portals. Y. Du, X. Zheng, and P. Huang are gratefully appreciated for downloading and processing the CMIP6 data. We thank all excellent scientists for their previous studies as materials necessary to compose this comprehensive article. Shanghai Ocean Conference of the Shanghai Jiao Tong University/School of Oceanography hosted a useful discussion for elaborating the paper. Three anonymous reviewers are gratefully appreciated for their useful comments and suggestions. J.M. was funded by the National Natural Science Foundation of China (NSFC) (41675070) and Shanghai Expert Development Fund (2017033). L.Z. was funded by the NSFC (41621064, 41530961, 41690121, and 41690120) and the IPOVAR Project (GASI-IPOVAI-01-02 and GASI-IPOVAI-02). G.R.F. was supported by base funds to NOAA/AOML's Physical Oceanography Division. X.Q. received support from the NSFC (41831175). J.Y. was funded by the NSFC (41706024). H.T. was supported by the KAKENHI Grants (18H01281, 18H03726, and 19H05704) of Japan Society for the Promotion of Science. J.L. was supported by the National Key Research and Development Program of China (2018YFA0605601). C.R.M. was funded by the U.S. National Science Foundation (AGS-1547912).

## Author contributions

J.M. initiated the whole paper and composed the abstract and "Important highlights of regional climate change" section. L.Z. was in charge of

"Introduction" and "IOD change" sections. G.R.F. was responsible for "Atlantic Niño and meridional mode" and "Discussion and outlook" sections. X.Q. drafted "The global monsoon system" and "Asian monsoon system" sections. J.Y. wrote "ENSO response" section. H.T. contributed to "Inter-decadal variability and global warming" section. J.L. summarized "Monsoon modulations by the ENSO" section. C.R.M. drafted "South American hydrology" section and revised the manuscript with help from X.G.

## Competing interests

The authors declare no competing interests.

## References

- Layton, D.F. & G. Brown. 2000. Heterogeneous preferences regarding global climate change. *Rev. Econ. Stat.* **82**: 616–624.
- Tingley, M.W., M.S. Koo, C. Moritz, *et al.* 2012. The push and pull of climate change causes heterogeneous shifts in avian elevational ranges. *Global Change Biol.* **18**: 3279–3290.
- Walther, G.-R. *et al.* 2002. Ecological responses to recent climate change. *Nature* **416**: 389–395.
- Moritz, C. & R. Agudo. 2013. The future of species under climate change: resilience or decline? *Science* **341**: 504–508.
- Hurrell, J., G.A. Meehl, D. Bader, *et al.* 2009. A unified modeling approach to climate system prediction. *Bull. Amer. Meteor. Soc.* **90**: 1819–1832.
- Martin, G.M., S.F. Milton, C.A. Senior, *et al.* 2010. Analysis and reduction of systematic errors through a seamless approach to modeling weather and climate. *J. Clim.* **23**: 5933–5957.
- Hoskins, B. 2013. The potential for skill across the range of the seamless weather-climate prediction problem: a stimulus for our science. *Q. J. R. Meteorol. Soc.* **139**: 573–584.
- Kennedy, J.J., N.A. Rayner, C.P. Atkinson, *et al.* 2019. An ensemble data set of sea-surface temperature change from 1850: the Met Office Hadley Centre HadSST.4.0.0.0 data set. *J. Geophys. Res.* **124**: 7719–7763.
- Fyfe, J.C., N.P. Gillett & F.W. Zwiers. 2013. Overestimated global warming over the past 20 years. *Nat. Clim. Change* **3**: 767–769.
- Delworth, T.L. & T.R. Knutson. 2000. Simulation of early 20th century global warming. *Science* **287**: 2246–2250.
- Deser, C., A.S. Phillips & M.A. Alexander. 2010. Twentieth century tropical sea surface temperature trends revisited. *Geophys. Res. Lett.* **37**: L10701.
- Wu, Z., N.E. Huang, J.M. Wallace, *et al.* 2011. On the time-varying trend in global-mean surface temperature. *Clim. Dyn.* **37**: 759–773.
- Harris, R.N. & D.S. Chapman. 2001. Mid-latitude (30°–60° N) climatic warming inferred by combining borehole temperatures with surface air temperatures. *Geophys. Res. Lett.* **28**: 747–750.

14. Fu, Q., C.M. Johanson, J.M. Wallace & T. Reichler. 2006. Enhanced mid-latitude tropospheric warming in satellite measurements. *Science* **312**: 1179–1179.
15. Frierson, D.M.W. 2006. Robust increases in midlatitude static stability in simulations of global warming. *Geophys. Res. Lett.* **33**: L24816.
16. Clarke, A.J. & A. Lebedev. 1996. Long-term change in the equatorial Pacific trade winds. *J. Clim.* **9**: 1020–1029.
17. Ma, J. & J.-Y. Yu. 2014. Linking centennial surface warming patterns in the equatorial Pacific to the relative strengths of the Walker and Hadley circulations. *J. Atmos. Sci.* **71**: 3454–3464.
18. Hansen, J., M. Sato, R. Ruedy, *et al.* 2006. Global temperature change. *Proc. Natl. Acad. Sci. USA* **103**: 14288–14293.
19. Kim, H.-M., P.J. Webster & J.A. Curry. 2009. Impact of shifting patterns of Pacific Ocean warming on north Atlantic tropical cyclones. *Science* **325**: 77–80.
20. Kosaka, Y. & S.-P. Xie. 2013. Recent global-warming hiatus tied to equatorial Pacific surface cooling. *Nature* **501**: 403–407.
21. McGregor, S., A. Timmermann, M.F. Stuecker, *et al.* 2014. Recent Walker circulation strengthening and Pacific cooling amplified by Atlantic warming. *Nat. Clim. Change* **4**: 888–892.
22. Vecchi, G.A. & B.J. Soden. 2007. Global warming and the weakening of the tropical circulation. *J. Clim.* **20**: 4316–4340.
23. DiNezio, P.N., A.C. Clement, G.A. Vecchi, *et al.* 2009. Climate response of the equatorial Pacific to global warming. *J. Clim.* **22**: 4873–4892.
24. Kao, H.-Y. & J.-Y. Yu. 2009. Contrasting Eastern-Pacific and Central-Pacific types of ENSO. *J. Clim.* **22**: 615–632.
25. Collins, M. *et al.* 2010. The impact of global warming on the tropical Pacific Ocean and El Niño. *Nat. Geosci.* **3**: 391–397.
26. Comiso, J.C. 2000. Variability and trends in Antarctic surface temperatures from *in situ* and satellite infrared measurements. *J. Clim.* **13**: 1674–1696.
27. Kwok, R. & J.C. Comiso. 2002. Spatial patterns of variability in Antarctic surface temperature: connections to the Southern Hemisphere Annular Mode and the Southern Oscillation. *Geophys. Res. Lett.* **29**: 50–51–50–54.
28. Ding, Q., E.J. Steig, D.S. Battisti & M. Kuttel. 2011. Winter warming in West Antarctica caused by central tropical Pacific warming. *Nat. Geosci.* **4**: 398–403.
29. Cai, W., G. Shi, T. Cowan, *et al.* 2005. The response of the Southern Annular Mode, the East Australian Current, and the southern mid-latitude ocean circulation to global warming. *Geophys. Res. Lett.* **32**: L23706.
30. Arblaster, J.M. & G.A. Meehl. 2006. Contributions of external forcings to Southern Annular Mode trends. *J. Clim.* **19**: 2896–2905.
31. Latif, M. & N.S. Keenlyside. 2009. El Niño/Southern Oscillation response to global warming. *Proc. Natl. Acad. Sci. USA* **106**: 20578–20583.
32. McGregor, H.V., M. Dima, H.W. Fischer & S. Mulitza. 2007. Rapid 20th-century increase in coastal upwelling off Northwest Africa. *Science* **315**: 637–639.
33. Roe, G.H. & M.B. Baker. 2007. Why is climate sensitivity so unpredictable? *Science* **318**: 629–632.
34. Andrews, T., J.M. Gregory, M.J. Webb & K.E. Taylor. 2012. Forcing, feedbacks and climate sensitivity in CMIP5 coupled atmosphere-ocean climate models. *Geophys. Res. Lett.* **39**: L09712.
35. Rogelj, J., M. Meinshausen & R. Knutti. 2012. Global warming under old and new scenarios using IPCC climate sensitivity range estimates. *Nat. Clim. Change* **2**: 248–253.
36. Tailleux, R. 2010. Entropy versus APE production: on the buoyancy power input in the oceans energy cycle. *Geophys. Res. Lett.* **37**. <https://doi.org/10.1029/2010GL044962>.
37. Pauluis, O. 2011. Water vapor and mechanical work: a comparison of Carnot and steam cycles. *J. Atmos. Sci.* **68**: 91–102.
38. Grotjahn, R. 2015. General circulation of the atmosphere | energy cycle. In *Encyclopedia of Atmospheric Sciences*. 2nd ed. G.R. North, J. Pyle & F. Zhang, Eds.: 51–64. Academic Press.
39. Emanuel, K.A., J.D. Neelin & C.S. Bretherton. 1994. On large-scale circulations in convecting atmospheres. *Q. J. R. Meteorol. Soc.* **120**: 1111–1143.
40. Neelin, J.D. & N. Zeng. 2000. A quasi-equilibrium tropical circulation model—formulation. *J. Atmos. Sci.* **57**: 1741–1766.
41. Yano, J.-I. & R.S. Plant. 2012. Convective quasi-equilibrium. *Rev. Geophys.* **50**: RG4004.
42. Held, I.M. & B.J. Soden. 2000. Water vapor feedback and global warming. *Annu. Rev. Energy Environ.* **25**: 441–475.
43. Soden, B.J., A.J. Broccoli & R.S. Hemler. 2004. On the use of cloud forcing to estimate cloud feedback. *J. Clim.* **17**: 3661–3665.
44. Dessler, A.E. 2010. A determination of the cloud feedback from climate variations over the past decade. *Science* **330**: 1523–1527.
45. Bony, S. *et al.* 2015. Clouds, circulation and climate sensitivity. *Nat. Geosci.* **8**: 261–268.
46. Tan, I., T. Storelvmo & M.D. Zelinka. 2016. Observational constraints on mixed-phase clouds imply higher climate sensitivity. *Science* **352**: 224–227.
47. Timmermann, A. *et al.* 2018. El Niño–Southern Oscillation complexity. *Nature* **559**: 535–545.
48. Held, I.M. & A.Y. Hou. 1980. Nonlinear axially symmetric circulations in a nearly inviscid atmosphere. *J. Atmos. Sci.* **37**: 515–533.
49. Ma, J., R. Chadwick, K.-H. Seo, *et al.* 2018. Responses of the tropical atmospheric circulation to climate change and connection to the hydrological cycle. *Annu. Rev. Earth Planet. Sci.* **46**: 549–580.
50. Chou, C. & J.D. Neelin. 2004. Mechanisms of global warming impacts on regional tropical precipitation. *J. Clim.* **17**: 2688–2701.
51. Held, I.M. & B.J. Soden. 2006. Robust responses of the hydrological cycle to global warming. *J. Clim.* **19**: 5686–5699.
52. Lu, J., G.A. Vecchi & T. Reichler. 2007. Expansion of the Hadley cell under global warming. *Geophys. Res. Lett.* **34**: L06805.
53. Ma, J., S.-P. Xie & Y. Kosaka. 2012. Mechanisms for tropical tropospheric circulation change in response to global warming. *J. Clim.* **25**: 2979–2994.

54. Ma, J. 2018. Rainfall and climate feedbacks. *Nat. Geosci.* **11**: 389.
55. Huang, P., D. Chen & J. Ying. 2017. Weakening of the tropical atmospheric circulation response to local sea surface temperature anomalies under global warming. *J. Clim.* **30**: 8149–8158.
56. Cai, W. *et al.* 2013. Projected response of the Indian Ocean Dipole to greenhouse warming. *Nat. Geosci.* **6**: 999–1007.
57. Lee, J.Y. & B. Wang. 2014. Future change of global monsoon in the CMIP5. *Clim. Dyn.* **42**: 101–119.
58. Kosaka, Y. & S.-P. Xie. 2016. The tropical Pacific as a key pacemaker of the variable rates of global warming. *Nat. Geosci.* **9**: 669–673.
59. Xie, S.-P. *et al.* 2015. Towards predictive understanding of regional climate change. *Nat. Clim. Change* **5**: 921–930.
60. Zhang, J., J. Che, J. Ma, *et al.* 2020. Surface warming patterns dominate the uncertainty in global water vapor plus lapse rate feedback. *Acta. Oceanol. Sin.* **39**: 81–89. <https://doi.org/10.1007/s13131-019-1531-2>.
61. Ma, J. & Q. Liu. 2018. Nonuniformity of climate change among ocean basins on the background of global warming. In *10000 Selected Problems in Sciences—Ocean Science*. H.S. Guan, J.P. Zhao *et al.*, Eds.:1089–1093. Beijing: Science Press. (In Chinese).
62. Ma, J. & S.-P. Xie. 2013. Regional patterns of sea surface temperature change: a source of uncertainty in future projections of precipitation and atmospheric circulation. *J. Clim.* **26**: 2482–2501.
63. Xie, S.-P., C. Deser, G.A. Vecchi, *et al.* 2010. Global warming pattern formation: sea surface temperature and rainfall. *J. Clim.* **23**: 966–986.
64. Chou, C., J.C.H. Chiang, C.W. Lan, *et al.* 2013. Increase in the range between wet and dry season precipitation. *Nat. Geosci.* **6**: 263–267.
65. Giannini, A., S. Salack, T. Lodoun, *et al.* 2013. A unifying view of climate change in the Sahel linking intra-seasonal, interannual and longer time scales. *Environ. Res. Lett.* **8**: 024010.
66. Chadwick, R. 2016. Which aspects of CO<sub>2</sub> forcing and SST warming cause most uncertainty in projections of tropical rainfall change over land and ocean? *J. Clim.* **29**: 2493–2509.
67. O’Gorman, P.A. & C.J. Muller. 2010. How closely do changes in surface and column water vapor follow Clausius-Clapeyron scaling in climate change simulations? *Environ. Res. Lett.* **5**: 025207.
68. Lucas, C., B. Timbal & H. Nguyen. 2014. The expanding tropics: a critical assessment of the observational and modeling studies. *WIREs Clim. Change* **5**: 89–112.
69. Wang, Y., J.H. Jiang & H. Su. 2015. Atmospheric responses to the redistribution of anthropogenic aerosols. *J. Geophys. Res. Atmos.* **120**: 9625–9641.
70. Voigt, A. & T.A. Shaw. 2015. Circulation response to warming shaped by radiative changes of clouds and water vapor. *Nat. Geosci.* **8**: 102–106.
71. Chen, G., J. Lu & D.M.W. Frierson. 2008. Phase speed spectra and the latitude of surface westerlies: interannual variability and the global warming trend. *J. Clim.* **21**: 5942–5959.
72. Kidston, J. *et al.* 2015. Stratospheric influence on tropospheric jet streams, storm tracks and surface weather. *Nat. Geosci.* **8**: 433–440.
73. Chou, C., T.-C. Wu & P.-H. Tan. 2013. Changes in gross moist stability in the tropics under global warming. *Clim. Dyn.* **41**: 2481–2496.
74. Vecchi, G.A., B.J. Soden, A.T. Wittenberg, *et al.* 2006. Weakening of tropical Pacific atmospheric circulation due to anthropogenic forcing. *Nature* **441**: 73–76.
75. Ma, J., G.R. Foltz, B.J. Soden, *et al.* 2016. Will surface winds weaken in response to global warming? *Environ. Res. Lett.* **11**: 124012.
76. Wentz, F.J., L. Ricciardulli, K. Hilburn & C. Mears. 2007. How much more rain will global warming bring? *Science* **317**: 233–235.
77. Knutson, T.R. & S. Manabe. 1995. Time-mean response over the tropical Pacific to increased CO<sub>2</sub> in a coupled ocean-atmosphere model. *J. Clim.* **8**: 2181–2199.
78. Neelin, J.D., C. Chou & H. Su. 2003. Tropical drought regions in global warming and El Niño teleconnections. *Geophys. Res. Lett.* **30**: 2275.
79. Chadwick, R., I. Boutle & G. Martin. 2013. Spatial patterns of precipitation change in CMIP5: why the rich do not get richer in the tropics. *J. Clim.* **26**: 3803–3822.
80. Johnson, N.C. & S.-P. Xie. 2010. Changes in the sea surface temperature threshold for tropical convection. *Nat. Geosci.* **3**: 842–845.
81. Lu, J. & B. Zhao. 2012. The role of oceanic feedback in the climate response to doubling CO<sub>2</sub>. *J. Clim.* **25**: 7544–7563.
82. Liu, Z., S. Vavrus, F. He, *et al.* 2005. Rethinking tropical ocean response to global warming: the enhanced equatorial warming. *J. Clim.* **18**: 4684–4700.
83. Mitras, C.M. & A. Clement. 2006. Recent behavior of the Hadley cell and tropical thermodynamics in climate models and reanalyses. *Geophys. Res. Lett.* **33**: L01810.
84. Solomon, A. & M. Newman. 2012. Reconciling disparate twentieth-century Indo-Pacific ocean temperature trends in the instrumental record. *Nat. Clim. Change* **2**: 691–699.
85. Eyring, V., S. Bony, G.A. Meehl, *et al.* 2016. Overview of the Coupled Model Intercomparison Project Phase 6 (CMIP6) experimental design and organization. *Geosci. Model Dev.* **9**: 1937–1958.
86. Cai, W., A. Santoso, G.J. Wang, *et al.* 2014. Increased frequency of extreme Indian Ocean dipole events due to greenhouse warming. *Nature* **510**: 254–258.
87. Li, G., S.-P. Xie & Y. Du. 2016. A robust but spurious pattern of climate change in model projections over the tropical Indian Ocean. *J. Clim.* **29**: 5589–5608.
88. Wu, L.-X., W.-J. Cai, L.-P. Zhang, *et al.* 2012. Enhanced warming over the global subtropical western boundary currents. *Nat. Clim. Change* **2**: 161–166.
89. Cornwall, W. 2018. In hot water. *Science* **363**: 442–445.
90. Oliver, E.C., J.A. Benthuisen, N.L. Bindoff, *et al.* 2017. The unprecedented 2015/16 Tasman Sea marine heatwave. *Nat. Commun.* **8**: 16101.
91. Cheng, L.J., J. Zhu, J. Abraham, *et al.* 2019. 2018 Continues record global ocean warming. *Adv. Atmos. Sci.* **36**: 249–252.

92. Xu, L., S.-P. Xie & Q. Liu. 2012. Mode water ventilation and subtropical countercurrent over the North Pacific in CMIP5 simulations and future projections. *J. Geophys. Res.* **117**: C12009.
93. Wang, G., S.-P. Xie, R.-X. Huang, *et al.* 2015. Robust warming pattern of global subtropical oceans and its mechanism. *J. Clim.* **28**: 8574–8584.
94. Delworth, T.L., F. Zeng, G.A. Vecchi, *et al.* 2016. The North Atlantic Oscillation as a driver of rapid climate change in the Northern Hemisphere. *Nat. Geosci.* **9**: 509–512.
95. Jackson, L.C., K.A. Peterson, C.D. Roberts, *et al.* 2016. Recent slowing of Atlantic Overturning Circulation as a recovery from earlier strengthening. *Nat. Geosci.* **9**: 518–522.
96. Abram, N. *et al.* 2019. IPCC special report on the ocean and cryosphere in a changing climate. Accessed December 15, 2019. <https://www.ipcc.ch/srocc/>.
97. Chen, X. & K.K. Tung. 2014. Varying planetary heat sink led to global-warming slowdown and acceleration. *Science* **345**: 897–903.
98. Fedorov, A.V. & S.G. Philander. 2000. Is El Niño changing? *Science* **288**: 1997–2002.
99. Stevenson, S.L. 2012. Significant changes to ENSO strength and impacts in the twenty-first century: results from CMIP5. *Geophys. Res. Lett.* **39**: L17703.
100. Cai, W. *et al.* 2014. Increasing frequency of extreme El Niño events due to greenhouse warming. *Nat. Clim. Change* **4**: 111–116.
101. Cai, W. *et al.* 2015. ENSO and greenhouse warming. *Nat. Clim. Change* **5**: 849–859.
102. Cai, W. *et al.* 2015. Increased frequency of extreme La Niña events under greenhouse warming. *Nat. Clim. Change* **5**: 132–137.
103. Meehl, G.A. *et al.* 2007. *Global climate projections*. Climate Change 2007: The Physical Science Basis. S. Solomon *et al.*, Eds.: 747–845. Cambridge: Cambridge University Press.
104. Christensen, J.H. *et al.* 2013. Climate phenomena and their relevance for future regional climate change. In *Climate Change 2013: The Physical Science Basis*. T.F. Stocker *et al.*, Eds.: 1217–1308. Cambridge: Cambridge University Press.
105. Power, S., F. Delage, C. Chung, *et al.* 2013. Robust twenty-first-century projections of El Niño and related precipitation variability. *Nature* **502**: 541–545.
106. Chang, P., R. Saravanan, L. Ji & G.C. Hegerl. 2000. The effect of local sea surface temperatures on atmospheric circulation over the tropical Atlantic sector. *J. Clim.* **13**: 2195–2216.
107. Deser, C., M.A. Alexander, S.-P. Xie & A.S. Phillips. 2010. Sea surface temperature variability: patterns and mechanisms. *Annu. Rev. Mar. Sci.* **2**: 115–143.
108. Kang, I.-S. & J.-S. Kug. 2002. El Niño and La Niña sea surface temperature anomalies: asymmetry characteristics associated with their wind stress anomalies. *J. Geophys. Res. Atmos.* **107**: ACL 1-1-ACL 1-10.
109. Kim, D., J.-S. Kug, I.-S. Kang, *et al.* 2008. Tropical Pacific impacts of convective momentum transport in the SNU coupled GCM. *Clim. Dyn.* **31**: 213–226.
110. Watanabe, M., J.-S. Kug, F.-F. Jin, *et al.* 2012. Uncertainty in the ENSO amplitude change from the past to the future. *Geophys. Res. Lett.* **39**: L20703.
111. Ying, J., P. Huang, T. Lian & D. Chen. 2019. Intermodel uncertainty in the change of ENSO's amplitude under global warming: role of the response of atmospheric circulation to SST anomalies. *J. Clim.* **32**: 369–383.
112. Graham, N.E. & T.P. Barnett. 1987. Sea surface temperature, surface wind divergence, and convection over tropical oceans. *Science* **238**: 657–659.
113. Bhat, G.S., J. Srinivasan & S. Gadgil. 1996. Tropical deep convection, convective available potential energy and sea surface temperature. *J. Meteorol. Soc. Jpn. Ser. II* **74**: 155–166.
114. He, J., N.C. Johnson, G.A. Vecchi, *et al.* 2018. Precipitation sensitivity to local variations in tropical sea surface temperature. *J. Clim.* **31**: 9225–9238.
115. Ying, J., P. Huang & R. Huang. 2016. Evaluating the formation mechanisms of the equatorial Pacific SST warming pattern in CMIP5 models. *Adv. Atmos. Sci.* **33**: 433–441.
116. Huang, P. & J. Ying. 2015. A multimodel ensemble pattern regression method to correct the tropical Pacific SST change patterns under global warming. *J. Clim.* **28**: 4706–4723.
117. Zheng, X.-T., S.-P. Xie, L.-H. Lv & Z.-Q. Zhou. 2016. Intermodel uncertainty in ENSO amplitude change tied to Pacific Ocean warming pattern. *J. Clim.* **29**: 7265–7279.
118. Chen, L., T. Li, Y. Yu & S.K. Behera. 2017. A possible explanation for the divergent projection of ENSO amplitude change under global warming. *Clim. Dyn.* **49**: 3799–3811.
119. Ying, J., P. Huang, T. Lian & H. Tan. 2019. Understanding the effect of an excessive cold tongue bias on projecting the tropical Pacific SST warming pattern in CMIP5 models. *Clim. Dyn.* **52**: 1805–1818.
120. Li, G., S.-P. Xie, Y. Du & Y. Luo. 2016. Effects of excessive equatorial cold tongue bias on the projections of tropical Pacific climate change. Part I: the warming pattern in CMIP5 multi-model ensemble. *Clim. Dyn.* **47**: 1–15.
121. Cai, W. *et al.* 2018. Increased variability of eastern Pacific El Niño under greenhouse warming. *Nature* **564**: 201–206.
122. Philip, S. & G.J. van Oldenborgh. 2006. Shifts in ENSO coupling processes under global warming. *Geophys. Res. Lett.* **33**: L11704.
123. DiNezio, P.N., B.P. Kirtman, A.C. Clement, *et al.* 2012. Mean climate controls on the simulated response of ENSO to increasing greenhouse gases. *J. Clim.* **25**: 7399–7420.
124. Kim, S.T., W. Cai, F.-F. Jin, *et al.* 2014. Response of El Niño sea surface temperature variability to greenhouse warming. *Nat. Clim. Change* **4**: 786–790.
125. Yeh, S.-W., J.-S. Kug, B. Dewitte, *et al.* 2009. El Niño in a changing climate. *Nature* **461**: 511–514.
126. Saji, N.H., B.N. Goswami, P.N. Vinayachandran & T. Yamagata. 1999. A dipole mode in the tropical Indian Ocean. *Nature* **401**: 360–363.
127. Webster, P.J., A.M. Moore, J.P. Loschnigg & R.R. Leben. 1999. Coupled ocean–atmosphere dynamics in the Indian Ocean during 1997–98. *Nature* **401**: 356–360.
128. Izumo, T. *et al.* 2010. Influence of the state of the Indian Ocean Dipole on the following year's El Niño. *Nat. Geosci.* **3**: 168–172.
129. Ihara, C., Y. Kushnir & M.A. Cane. 2008. Warming trend of the Indian Ocean SST and Indian Ocean Dipole from 1880 to 2004. *J. Clim.* **21**: 2035–2046.

130. Cai, W., T. Cowan & A. Sullivan. 2009. Recent unprecedented skewness towards positive Indian Ocean Dipole occurrences and its impact on Australian rainfall. *Geophys. Res. Lett.* **36**: L11705.
131. Roxy, M.K., K. Ritika, P. Terray & S. Masson. 2014. The curious case of Indian Ocean warming. *J. Clim.* **27**: 8501–8509.
132. Yang, J., Q. Liu, Z. Liu, *et al.* 2009. Basin mode of Indian Ocean sea surface temperature and Northern Hemisphere circumglobal teleconnection. *Geophys. Res. Lett.* **36**. <https://doi.org/10.1029/2009GL039559>.
133. Cai, W., A. Sullivan & T. Cowan. 2009. Climate change contributes to more frequent consecutive positive Indian Ocean Dipole events. *Geophys. Res. Lett.* **36**: L23704.
134. Abram, N.J., M.K. Gagan, J.E. Cole, *et al.* 2008. Recent intensification of tropical climate variability in the Indian Ocean. *Nat. Geosci.* **1**: 849–853.
135. Nakamura, N., H. Kayanne, H. Iijima, *et al.* 2009. Mode shift in the Indian Ocean climate under global warming stress. *Geophys. Res. Lett.* **36**: L23708.
136. Du, Y. & S.-P. Xie. 2008. Role of atmospheric adjustments in the tropical Indian Ocean warming during the 20th century in climate models. *Geophys. Res. Lett.* **35**: L08712.
137. Ashok, K., W.-L. Chan, T. Motoi & T. Yamagata. 2004. Decadal variability of the Indian Ocean dipole. *Geophys. Res. Lett.* **31**: 1–4.
138. Zheng, X.-T., S.-P. Xie, G.A. Vecchi, *et al.* 2010. Indian Ocean Dipole response to global warming: analysis of ocean–atmospheric feedbacks in a coupled model. *J. Clim.* **23**: 1240–1253.
139. Zheng, X.-T., S.-P. Xie, Y. Du, *et al.* 2013. Indian Ocean Dipole response to global warming in the CMIP5 multi-model ensemble. *J. Clim.* **26**: 6067–6080.
140. Meyers, G., P. McIntosh, L. Pigot & M. Pook. 2007. The years of El Niño, La Niña, and interactions with the tropical Indian Ocean. *J. Clim.* **20**: 2872–2880.
141. Chen, D. 2011. Indo-Pacific Tripole: an intrinsic mode of tropical climate variability. *Adv. Geosci.* **24**: 1–18.
142. Zhou, L., R. Murtugudde & M. Jochum. 2008. Seasonal influence of Indonesian throughflow in the southwestern Indian Ocean. *J. Phys. Oceanogr.* **38**: 1529–1541.
143. Mayer, M., M.A. Balmaseda & L. Haimberger. 2018. Unprecedented 2015/2016 Indo-Pacific heat transfer speeds up tropical Pacific heat recharge. *Geophys. Res. Lett.* **45**: 3274–3284.
144. Liu, W., S.-P. Xie & J. Lu. 2016. Tracking ocean heat uptake during the surface warming hiatus. *Nat. Commun.* **7**: 10926.
145. Gordon, A.L., B.A. Huber, E.J. Metzger, *et al.* 2012. South China Sea throughflow impact on the Indonesian throughflow. *Geophys. Res. Lett.* **39**: L11602.
146. Tillinger, D. & A.L. Gordon. 2010. Transport weighted temperature and internal energy transport of the Indonesian throughflow. *Dyn. Atmos. Oceans* **50**: 224–232.
147. Qu, T.-D., Y. Du & H. Sasaki. 2006. South China Sea throughflow: a heat and freshwater conveyor. *Geophys. Res. Lett.* **33**: 430–452.
148. Gordon, A.L., R.D. Susanto & K. Vranes. 2003. Cool Indonesian throughflow as a consequence of restricted surface layer flow. *Nature* **425**: 824–828.
149. Zhou, L. & R. Murtugudde. 2009. Influence of the Makassar Strait throughflow and winds over the southeastern Indian Ocean on the southwestern Indian Ocean SST variability. *Adv. Geosci.* **12**: 71–86.
150. Song, Q. & A.L. Gordon. 2004. Significance of the vertical profile of the Indonesian throughflow transport to the Indian Ocean. *Geophys. Res. Lett.* **31**: L16307.
151. Zhou, L., R. Murtugudde & M. Jochum. 2008. Dynamics of the intraseasonal oscillations in the Indian Ocean South Equatorial Current. *J. Phys. Oceanogr.* **38**: 121–132.
152. Song, Q., A.L. Gordon & M. Visbeck. 2004. Spreading of the Indonesian throughflow in the Indian Ocean. *J. Phys. Oceanogr.* **34**: 772–792.
153. Yuan, D., X. Hu, P. Xu, *et al.* 2018. The IOD-ENSO precursory teleconnection over the tropical Indo-Pacific Ocean: dynamics and long-term trends under global warming. *J. Oceanol. Limnol.* **36**: 4–19.
154. Kug, J.-S. & I.-S. Kang. 2006. Interactive feedback between ENSO and the Indian Ocean. *J. Clim.* **19**: 1784–1801.
155. Luo, J.-J., R. Zhang, S.K. Behera, *et al.* 2010. Interaction between El Niño and extreme Indian Ocean Dipole. *J. Clim.* **23**: 726–742.
156. Tokinaga, H. & S.-P. Xie. 2011. Weakening of the equatorial Atlantic cold tongue over the past six decades. *Nat. Geosci.* **4**: 222–226.
157. Enfield, D.B., A.M. Mestas-Nuñez & P.J. Trimble. 2001. The Atlantic multidecadal oscillations and its relation to rainfall and river flows in the continental U.S. *Geophys. Res. Lett.* **28**: 2077–2080.
158. Servain, J., G. Caniaux, Y.K. Kouadio, *et al.* 2014. Recent climatic trends in the tropical Atlantic. *Clim. Dyn.* **41**: 3071–3089.
159. Lübbecke, J.F., J.V. Durgadoo & A. Biastoch. 2015. Contribution of increased Agulhas leakage to tropical Atlantic warming. *J. Clim.* **28**: 9697–9706.
160. Zebiak, S.E. 1993. Air–sea interaction in the equatorial Atlantic region. *J. Clim.* **6**: 1567–1586.
161. Lübbecke, J.F., B. Rodriguez-Fonseca, I. Richter, *et al.* 2018. Equatorial Atlantic variability—modes, mechanisms, and global teleconnections. *Wires Clim. Change* **9**: e527.
162. Keenlyside, N.S. & M. Latif. 2007. Understanding equatorial Atlantic interannual variability. *J. Clim.* **20**: 131–142.
163. Nobre, P. & J. Shukla. 1996. Variations of sea surface temperature, wind stress and rainfall over the tropical Atlantic and South America. *J. Clim.* **9**: 2464–2479.
164. Chiang, J.C.H. & D.J. Vimont. 2004. Analogous Pacific and Atlantic meridional modes of tropical atmosphere–ocean variability. *J. Clim.* **17**: 4143–4158.
165. Chiang, J.C.H., Y. Kushnir & A. Giannini. 2002. Deconstructing Atlantic intertropical convergence zone variability: influence of the local cross-equatorial sea surface temperature gradient and remote forcing from the eastern equatorial Pacific. *J. Geophys. Res.* **107**: ACL 3-1-ACL 3-19.
166. Czaja, A., P. Van der Vaart & J. Marshall. 2002. A diagnostic study of the role of remote forcing in tropical Atlantic variability. *J. Clim.* **15**: 3280–3290.
167. Xie, S.-P. 1999. A dynamic ocean-atmosphere model of the tropical Atlantic decadal variability. *J. Clim.* **12**: 64–70.

168. Zeng, N., J.H. Yoon, J.A. Marengo, *et al.* 2008. Causes and impacts of the 2005 Amazon drought. *Environ. Res. Lett.* **3**: 014002.
169. Lewis, S.L., P.M. Brando, O.L. Phillips, *et al.* 2011. The 2010 Amazon drought. *Science* **331**: 554–555.
170. Foltz, G.R., M.J. McPhaden & R. Lumpkin. 2012. A strong Atlantic meridional mode event in 2009: the role of mixed layer dynamics. *J. Clim.* **25**: 363–380.
171. Brito, S.S.B., A.P.M.A. Cunha, C.C. Cunningham, *et al.* 2018. Frequency, duration and severity of drought in the Semiarid Northeast Brazil region. *Int. J. Climatol.* **38**: 517–529.
172. Foltz, G.R., P. Brandt, I. Richter, *et al.* 2019. The Tropical Atlantic observing system. *Front. Mar. Sci.* **6**: 206.
173. Kossin, J.P. & D.J. Vimont. 2007. A more general framework for understanding Atlantic hurricane variability and trends. *Bull. Am. Meteorol. Soc.* **88**: 1767–1781.
174. Losada, T., B. Rodríguez-Fonseca, I. Polo, *et al.* 2010. Tropical response to the Atlantic Equatorial mode: aGCM multimodel approach. *Clim. Dyn.* **35**: 45–52.
175. Keenlyside, N.S., H. Ding & M. Latif. 2013. Potential of equatorial Atlantic variability to enhance El Niño prediction. *Geophys. Res. Lett.* **40**: 2278–2283.
176. Kucharski, F., A. Bracco, J.H. Yoo & F. Molteni. 2008. Atlantic forced component of the Indian monsoon interannual variability. *Geophys. Res. Lett.* **35**: L04706.
177. Wu, L., F. He, Z. Liu & C. Li. 2007. Atmospheric teleconnections of tropical Atlantic variability: interhemispheric, tropical-extratropical, and cross-basin interactions. *J. Clim.* **20**: 856–870.
178. Ham, Y.-G., J.-S. Kug, J.-Y. Park & F.-F. Jin. 2013. Sea surface temperature in the north tropical Atlantic as a trigger for El Niño/Southern Oscillation events. *Nat. Geosci.* **6**: 112–116.
179. Ham, Y.-G., J.-S. Kug & J.-Y. Park. 2013. Two distinct roles of Atlantic SSTs in ENSO variability: north tropical Atlantic SST and Atlantic Niño. *Geophys. Res. Lett.* **40**: 4012–4017.
180. Ashfaq, M., C.B. Skinner & N.S. Diffenbaugh. 2011. Influence of SST biases on future climate change projections. *Clim. Dyn.* **36**: 1303–1319.
181. Richter, I. 2015. Climate model biases in the eastern tropical oceans: causes, impacts and ways forward. *WIREs Clim. Change* **6**: 345–358.
182. Mohino, E. & T. Losada. 2015. Impacts of the Atlantic Equatorial Mode in a warmer climate. *Clim. Dyn.* **45**: 2255–2271.
183. Wang, B. & Q. Ding. 2008. Global monsoon: dominant mode of annual variation in the tropics. *Dyn. Atmos. Oceans* **44**: 165–183.
184. Trenberth, K.E., D.P. Stepaniak & J.M. Caron. 2000. The global monsoon as seen through the divergent atmospheric circulation. *J. Clim.* **13**: 3969–3993.
185. Hsu, P., T. Li, H. Murakami & A. Kitoh. 2013. Future change of the global monsoon revealed from 19 CMIP5 models. *J. Geophys. Res.* **118**: 1247–1260.
186. Qu, X. & G. Huang. 2019. Global monsoon changes under the Paris Agreement Temperature Goals in CESM1(CAM5). *Adv. Atmos. Sci.* **36**: 279–291.
187. Kitoh, A., H. Endo, K.K. Kumar, *et al.* 2013. Monsoons in a changing world: a regional perspective in a global context. *J. Geophys. Res.* **118**: 3053–3065.
188. Endo, H. & A. Kitoh. 2014. Thermodynamic and dynamic effects on regional monsoon rainfall changes in a warmer climate. *Geo. Res. Lett.* **41**: 1704–1711.
189. Hsu, P.C., T. Li & B. Wang. 2011. Trends in global monsoon area and precipitation over the past 30 years. *Geophys. Res. Lett.* **38**: L08701.
190. Boos, W.R. & Z. Kuang. 2010. Dominant control of the South Asian monsoon by orographic insulation versus plateau heating. *Nature* **463**: 218–222.
191. Wu, G., Y. Liu, B. He, *et al.* 2012. Thermal controls on the Asian Summer Monsoon. *Sci. Rep.* **2**: 404.
192. Liu, Y., B. Hoskins & M. Blackburn. 2007. Impact of Tibetan orography and heating on the summer flow over Asia. *J. Meteor. Soc. Japan* **85**: 1–19.
193. Lee, J.Y., B. Wang, K.H. Seo, *et al.* 2015. Effects of mountain uplift on global monsoon precipitation. *Asia-Pac. J. Atmos. Sci.* **51**: 275–290.
194. Endo, H., A. Kitoh & H. Ueda. 2018. A unique feature of the Asian summer monsoon response to global warming: the role of different land–sea thermal contrast change between the lower and upper troposphere. *SOLA* **14**: 57–63.
195. Sooraj, K.P., P. Terray & M. Mujumdar. 2015. Global warming and the weakening of the Asian summer monsoon circulation: assessments from the CMIP5 models. *Clim. Dyn.* **45**: 233–252.
196. Ma, J. & J.-Y. Yu. 2014. Paradox in South Asian summer monsoon circulation change: lower tropospheric strengthening and upper tropospheric weakening. *Geophys. Res. Lett.* **41**: 2934–2940.
197. He, C., Z. Wang, T. Zhou & T. Li. 2019. Enhanced latent heating over Tibetan Plateau as a key for the enhanced East Asian summer monsoon circulation under a warming climate. *J. Clim.* **32**: 3373–3388.
198. Ueda, H., A. Iwai, K. Kuwako & M.E. Hori. 2006. Impact of anthropogenic forcing on the Asian summer monsoon as simulated by eight GCMs. *Geophys. Res. Lett.* **33**: L06703.
199. Li, X. & M. Ting. 2017. Understanding the Asian summer monsoon response to greenhouse warming: the relative roles of direct radiative forcing and sea surface temperature change. *Clim. Dyn.* **49**: 2863–2880.
200. de Barros Soares, D., H. Lee, P.C. Loikith, *et al.* 2017. Can significant trends be detected in surface air temperature and precipitation over South America in recent decades? *Int. J. Climatol.* **37**: 1483–1493.
201. Jones, C. & L.M.V. Carvalho. 2013. Climate Change in the South American Monsoon System: present Climate and CMIP5 Projections. *J. Clim.* **26**: 6660–6678.
202. Barkhordarian, A., H. von Storch, E. Zorita, *et al.* 2017. Observed warming over northern South America has an anthropogenic origin. *Clim. Dyn.* **51**: 1901–1914.
203. Barkhordarian, A., H. von Storch, A. Behrangi, *et al.* 2018. Simultaneous regional detection of land-use changes and elevated GHG levels: the case of spring precipitation in tropical South America. *Geophys. Res. Lett.* **45**: 6262–6271.

204. Barkhordarian, A., S.S. Saatchi, A. Behrangi, *et al.* 2019. The impact of anthropogenic forcings on the rise of vapor pressure deficit over the Amazon. *Nat. Sci. Rep.* **9**: 15331.
205. Mohtadi, M., M. Prange & S. Steinke. 2016. Palaeoclimatic insights into forcing and response of monsoon rainfall. *Nature* **533**: 191–199.
206. Wang, P.-X., B. Wang, H. Cheng, *et al.* 2014. The global monsoon across timescales: coherent variability of regional monsoons. *Clim. Past* **10**: 2007–2052.
207. Wang, P.-X., B. Wang, H. Cheng, *et al.* 2017. The global monsoon across time scales: mechanisms and outstanding issues. *Earth-Sci. Rev.* **174**: 84–121.
208. Wang, B., R. Wu & T. Li. 2003. Atmosphere–warm ocean interaction and its impacts on Asian–Australian monsoon variation. *J. Clim.* **16**: 1195–1211.
209. Wang, B., J. Liu, H.J. Kim, *et al.* 2012. Recent change of the global monsoon precipitation (1979–2008). *Clim. Dyn.* **39**: 1123–1135.
210. Diaz, H.F., M.P. Hoerling & J.K. Eischeid. 2001. ENSO variability, teleconnections and climate change. *Int. J. Climatol.* **21**: 1845–1862.
211. Kumar, K.K., B. Rajagopalan & M.A. Cane. 1999. On the weakening relationship between the Indian monsoon and ENSO. *Science* **284**: 2156–2159.
212. Wang, B., J. Yang, T. Zhou, *et al.* 2008. Interdecadal changes in the major modes of Asian–Australian monsoon variability: strengthening relationship with ENSO since the late 1970s. *J. Clim.* **21**: 1771–1789.
213. Xie, S.-P., Y. Du, G. Huang, *et al.* 2010. Decadal shift in El Niño influences on Indo-western Pacific and East Asian climate in the 1970s. *J. Clim.* **23**: 3352–3368.
214. McCabe, G.J. & M.D. Dettinger. 1999. Decadal variations in the strength of ENSO teleconnections with precipitation in the western United States. *Int. J. Climatol.* **19**: 1399–1410.
215. Krishnamurthy, V. & B.N. Goswami. 2000. Indian monsoon–ENSO relationship on interdecadal timescale. *J. Clim.* **13**: 579–595.
216. Gershunov, A., N. Schneider & T. Barnett. 2001. Low-frequency modulation of the ENSO–Indian monsoon rainfall relationship: signal or noise? *J. Clim.* **14**: 2486–2492.
217. Li, J., S.-P. Xie, E.R. Cook, *et al.* 2013. El Niño modulations over the past seven centuries. *Nat. Clim. Change* **3**: 822–826.
218. Zhang, X., M. Wu, Y. Liu, *et al.* 2018. The relationship between the east Asian summer monsoon and El Niño–Southern Oscillation revealed by reconstructions and a control simulation for millennium. *Quat. Int.* **493**: 106–113.
219. Shi, H. & B. Wang. 2019. How does the Asian summer precipitation–ENSO relationship change over the past 544 years? *Clim. Dyn.* **52**: 4583–4598.
220. Ashok, K., S.K. Behera, S.A. Rao, *et al.* 2007. El Niño Modoki and its possible teleconnection. *J. Geophys. Res.* **112**: C11007.
221. Weng, H., K. Ashok, S.K. Behera, *et al.* 2007. Impacts of recent El Niño Modoki on dry/wet conditions in the Pacific rim during boreal summer. *Clim. Dyn.* **29**: 113–129.
222. Ashok, K., Z. Guan & T. Yamagata. 2001. Impact of the Indian Ocean dipole on the relationship between the Indian monsoon rainfall and ENSO. *Geophys. Res. Lett.* **28**: 4499–4502.
223. Vera, C.S., W. Higgins, J. Amador, *et al.* 2006. Toward a unified view of the American monsoon systems. *J. Clim.* **19**: 4977–5000.
224. Wang, B., J. Liu, H.J. Kim, *et al.* 2013. Northern Hemisphere summer monsoon intensified by mega-El Niño/southern oscillation and Atlantic multidecadal oscillation. *Proc. Natl. Acad. Sci. USA* **110**: 5347–5352.
225. Li, J., S.-P. Xie & E.R. Cook. 2014. El Niño phases embedded in Asian and North American drought reconstructions. *Quat. Sci. Rev.* **85**: 20–34.
226. Jourdain, N.C., A.S. Gupta, A.S. Taschetto, *et al.* 2013. The indo-Australian monsoon and its relationship to ENSO and IOD in reanalysis data and the CMIP3/CMIP5 simulations. *Clim. Dyn.* **41**: 3073–3102.
227. Roy, L., A.S. Gagnon & D. Siingh. 2019. Evaluating ENSO teleconnections using observations and CMIP5 models. *Theor. Appl. Climatol.* **136**: 1085–1098.
228. Zhang, H.-M., J.H. Lawrimore, B. Huang, *et al.* 2019. The NOAA global surface temperature dataset version 5: employing improved data coverage and historical homogenization. *AGU Eos*. In press.
229. Lenssen, N.J.L., G.A. Schmidt, J.E. Hansen, *et al.* 2019. Improvements in the uncertainty model in the Goddard Institute for Space Studies Surface Temperature (GIS-TEMP) analysis. *J. Geophys. Res. Atmos.* **124**: 6307–6326.
230. Morice, C.P., J.J. Kennedy, N.A. Rayner & P.D. Jones. 2012. Quantifying uncertainties in global and regional temperature change using an ensemble of observational estimates: the HadCRUT4 data set. *J. Geophys. Res. Atmos.* **117**. <https://doi.org/10.1029/2011JD017187>.
231. Brönnimann, S. 2009. Early twentieth-century warming. *Nat. Geosci.* **2**: 735–736.
232. Myhre, G. *et al.* 2013. Anthropogenic and natural radiative forcing. In *Climate Change 2013: The Physical Science Basis*. T.F. Stocker *et al.*, Eds.:659–740. Cambridge: Cambridge University Press.
233. Vaughan, D.G. *et al.* 2013. Observations: cryosphere. In *Climate Change 2013: The Physical Science Basis*. T.F. Stocker *et al.*, Eds.:317–382. Cambridge: Cambridge University Press.
234. Shiogama, H., T. Nagashima, T. Yokohata, *et al.* 2006. Influence of volcanic activity and changes in solar irradiance on surface air temperatures in the early twentieth century. *Geophys. Res. Lett.* **33**: L09702.
235. Nozawa, T., T. Nagashima, H. Shiogama & S.A. Crooks. 2005. Detecting natural influence on surface air temperature change in the early twentieth century. *Geophys. Res. Lett.* **32**: L20719.
236. Min, S.K. & A. Hense. 2006. A Bayesian assessment of climate change using multimodel ensembles. Part I: global mean surface temperature. *J. Clim.* **19**: 3237–3256.
237. Andronova, N.G. & M.E. Schlesinger. 2000. Causes of global temperature changes during the 19th and 20th centuries. *Geophys. Res. Lett.* **27**: 2137–2140.
238. Ring, M.J., D. Lindner, E.F. Cross & M.E. Schlesinger. 2012. Causes of the global warming observed since the 19th century. *Atmos. Clim. Sci.* **2**: 401–415.

239. Shindell, D. & G. Faluvegi. 2009. Climate response to regional radiative forcing during the twentieth century. *Nat. Geosci.* **2**: 294–300.
240. Tokinaga, H., S.-P. Xie & H. Mukougawa. 2017. Early 20th-century Arctic warming intensified by Pacific and Atlantic multidecadal variability. *Proc. Natl Acad. Sci. USA* **114**: 6227–6232.
241. Svendsen, L., N. Keenlyside, I. Bethke, *et al.* 2018. Pacific contribution to the early twentieth-century warming in the Arctic. *Nat. Clim. Change* **8**: 793–797.
242. Meehl, G.A., J.M. Arblaster, J.T. Fasullo, *et al.* 2011. Model-based evidence of deep-ocean heat uptake during surface-temperature hiatus periods. *Nat. Clim. Change* **1**: 360–364.
243. England, M.H. *et al.* 2014. Recent intensification of wind-driven circulation in the Pacific and the ongoing warming hiatus. *Nat. Clim. Change* **4**: 222–227.
244. Meehl, G.A., H. Teng & J.M. Arblaster. 2014. Climate model simulations of the observed early-2000s hiatus of global warming. *Nat. Clim. Change* **4**: 898–902.
245. Schmidt, G.A., D.T. Shindell & K. Tsigaridis. 2014. Reconciling warming trends. *Nat. Geosci.* **7**: 158–160.
246. Santer, B.D. *et al.* 2014. Volcanic contribution to decadal changes in tropospheric temperature. *Nat. Geosci.* **7**: 185–189.
247. Trenberth, K. 2015. Has there been a hiatus? *Science* **349**: 691–692.
248. Dai, A., J.C. Fyfe, S.-P. Xie & X. Dai. 2015. Decadal modulation of global surface temperature by internal climate variability. *Nat. Clim. Change* **5**: 555–559.
249. Gleisner, H., P. Thejll, B. Christiansen & J.K. Nielsen. 2015. Recent global warming hiatus dominated by low-latitude temperature trends in surface and troposphere data. *Geophys. Res. Lett.* **42**: 510–517.
250. Yan, X.-H., T. Boyer, K. Trenberth, *et al.* 2016. The global warming hiatus: slowdown or redistribution? *Earth's Future* **4**: 472–482.
251. Drijfhout, S.S., A.T. Blaker, S.A. Josey, *et al.* 2014. Surface warming hiatus caused by increased heat uptake across multiple ocean basins. *Geophys. Res. Lett.* **41**: 7868–7874.
252. Meehl, G.A., A.-X. Hu, J.M. Arblaster, *et al.* 2013. Externally forced and internally generated decadal climate variability associated with the interdecadal Pacific oscillation. *J. Clim.* **26**: 7298–7310.
253. Li, X.-C., S.-P. Xie, S.T. Gille & C. Yoo. 2016. Atlantic-induced pan-tropical climate change over the past three decades. *Nat. Clim. Change* **6**: 275–279.
254. Steinman, B.A., M.E. Mann & S.K. Miller. 2015. Atlantic and Pacific multidecadal oscillations and Northern Hemisphere temperatures. *Science* **347**: 988–991.
255. Takahashi, C. & M. Watanabe. 2016. Pacific trade winds accelerated by aerosol forcing over the past two decades. *Nat. Clim. Change* **6**: 768–772.
256. Hua, W., A. Dai & M. Qin. 2018. Contributions of internal variability and external forcing to the recent Pacific decadal variations. *Geophys. Res. Lett.* **45**: 7084–7092.
257. Adler, R.F., G. Gu, M. Sapiano, *et al.* 2017. Global precipitation: means, variations and trends during the satellite era (1979–2014). *Surv. Geophys.* **38**: 679–699.
258. Kamae, Y., X. Li, S.-P. Xie & H. Ueda. 2017. Atlantic effects on recent decadal trends in global monsoon. *Clim. Dyn.* **49**: 3443–3455.
259. Karl, T.R. *et al.* 2015. Possible artifacts of data biases in the recent global surface warming hiatus. *Science* **348**: 1469–1472.
260. Rajaratnam, B., J. Romano, M. Tsiang & N.S. Diffenbaugh. 2015. Debunking the climate hiatus. *Clim. Change* **133**: 129–140.
261. Gregory, J.M. *et al.* 2016. The Flux-Anomaly-Forced Model Intercomparison Project (FAFMIP) contribution to CMIP6: investigation of sea-level and ocean climate change in response to CO<sub>2</sub> forcing. *Geosci. Model Dev.* **9**: 3993–4017.
262. Andrews, T. & M.J. Webb. 2018. The dependence of global cloud and lapse-rate feedbacks on the spatial structure of tropical Pacific warming. *J. Clim.* **31**: 641–654.
263. Ying, J. & P. Huang. 2016. Cloud–radiation feedback as a leading source of uncertainty in the tropical Pacific SST warming pattern in CMIP5 models. *J. Clim.* **29**: 3867–3881.